

UNCLASSIFIED

AD NUMBER

ADB004294

LIMITATION CHANGES

TO:

Approved for public release; distribution is unlimited.

FROM:

Distribution authorized to U.S. Gov't. agencies only; Test and Evaluation; MAR 1975. Other requests shall be referred to Air Force Avionics Lab., Wright-Patterson AFB, OH 45433.

AUTHORITY

AFAL ltr 4 Sep 1975

THIS PAGE IS UNCLASSIFIED

THIS REPORT HAS BEEN DELIMITED
AND CLEARED FOR PUBLIC RELEASE
UNDER DOD DIRECTIVE 5200.20 AND
NO RESTRICTIONS ARE IMPOSED UPON
ITS USE AND DISCLOSURE.

DISTRIBUTION STATEMENT A

APPROVED FOR PUBLIC RELEASE;
DISTRIBUTION UNLIMITED.

L
AFAL-TR-75-13

ADB004294

HIGH-POWER LOC LASERS: SYNTHESIS AND MODE CONTROL

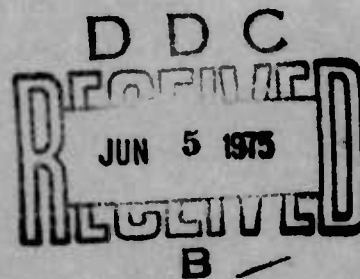
**H. F. LOCKWOOD
H. KRESSEL**

**RCA LABORATORIES
PRINCETON, NEW JERSEY 08540**

TECHNICAL REPORT AFAL-TR-75-13

MARCH 1975

FINAL REPORT FOR PERIOD 1 DECEMBER 1973 — 30 NOVEMBER 1974



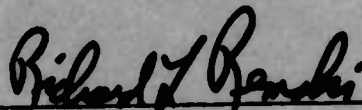
Distribution is limited to U.S. Government agencies only; test and evaluation results reported: January 1975. Other requests for this document must be referred to AFAL/TEO, Wright-Patterson AFB, Ohio 45433.

**AIR FORCE AVIONICS LABORATORY
AIR FORCE SYSTEMS COMMAND
WRIGHT-PATTERSON AIR FORCE BASE, OHIO 45433**

NOTICE

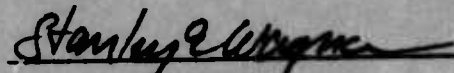
When Government drawings, specifications, or other data are used for any purpose other than in connection with a definitely related Government procurement operation, the United States Government thereby incurs no responsibility nor any obligation whatsoever; and the fact that the government may have formulated, furnished, or in any way supplied the said drawings, specifications, or other data, is not to be regarded by implication or otherwise as in any manner licensing the holder or any other person or corporation, or conveying any rights or permission to manufacture, use, or sell any patented invention that may in any way be related thereto.

The manuscript of this report was submitted by the authors on 10 January 1975. The Air Force Project Engineer is Mr. Robert L. Harris. This Final Report has been reviewed and is approved for publication.



RICHARD L. REMSKI
Act'g Chief
E-O Sources Group
Electro-Optics Device Branch
Electronic Technology Division

FOR THE DIRECTOR



STANLEY E. WAGNER
Act'g Chief
Electro-Optics Device Branch
Electronic Technology Division

Copies of this report should not be returned unless return is required by security considerations, contractual obligations, or notice on a specific document.

UNCLASSIFIED

SECURITY CLASSIFICATION OF THIS PAGE (When Data Entered)

REPORT DOCUMENTATION PAGE		READ INSTRUCTIONS BEFORE COMPLETING FORM
1. REPORT NUMBER AFAL-TR-75-13	2. GOVT ACCESSION NO.	3. RECIPIENT'S CATALOG NUMBER
4. TITLE (and Subtitle) HIGH-POWER LOC LASERS: SYNTHESIS AND MODE CONTROL		5. TYPE OF REPORT & PERIOD COVERED Final Report (12-1-73 to 11-30-74)
		6. PERFORMING ORG. REPORT NUMBER PRRL-75-CR-1
7. AUTHOR(s) Harry F. Lockwood and Henry Kressel		8. CONTRACT OR GRANT NUMBER(s) F33615-74-C-1016
9. PERFORMING ORGANIZATION NAME AND ADDRESS RCA Laboratories Princeton, New Jersey 08540		10. PROGRAM ELEMENT, PROJECT, TASK AREA & WORK UNIT NUMBERS Project No. 2001 Task No. 200101
11. CONTROLLING OFFICE NAME AND ADDRESS Air Force Avionics Laboratory Air Force Systems Command Wright-Patterson AFB, Ohio 45433		12. REPORT DATE March 1975
		13. NUMBER OF PAGES 47
14. MONITORING AGENCY NAME & ADDRESS (if different from Controlling Office)		15. SECURITY CLASS. (of this report) Unclassified
		15a. DECLASSIFICATION/DOWNGRADING SCHEDULE N/A
16. DISTRIBUTION STATEMENT (of this Report) Distribution is limited to U.S. Government agencies only; test and evaluation results reported: January 1975. Other requests for this document must be referred to AFAL/TEO, Wright-Patterson AFB, Ohio 45433.		
17. DISTRIBUTION STATEMENT (of the abstract entered in Block 20, if different from Report)		
18. SUPPLEMENTARY NOTES		
19. KEY WORDS (Continue on reverse side if necessary and identify by block number) High-power LOC lasers Heterojunction laser diodes Large optical cavity (LOC) lasers		
20. ABSTRACT (Continue on reverse side if necessary and identify by block number) Progress in the fabrication technology of GaAs and (AlGa)As heterojunction laser diodes made by liquid-phase epitaxy and in our theoretical understanding of laser diodes has permitted the design of sophisticated structures. Research interest has been on devices useful at room temperature for high peak power (pulsed) operation and reliable continuous operation. Both types of devices require low thermal and electrical resistance but other characteristics differ; e.g., high-power pulsed lasers need not have		

DD FORM 1473
1 JAN 73

EDITION OF 1 NOV 65 IS OBSOLETE

UNCLASSIFIED

SECURITY CLASSIFICATION OF THIS PAGE (When Data Entered)

UNCLASSIFIED

SECURITY CLASSIFICATION OF THIS PAGE(When Data Entered)

20.

very low threshold current densities but must withstand catastrophic degradation resulting from excessive optical flux density at the emitting facet, whereas cw lasers operate at low power (tens of milliwatts) and low threshold current densities to minimize thermal dissipation problems. The beam divergence in each type is low to reduce the external optical collimating system size.

Under this contract, we had the following primary technical goals: (1) Optimize structure for fundamental transverse mode operation with beam width (FWHM) of $\sim 25^\circ$ - 30° , (2) Demonstrate efficient operation at *elevated* temperatures (75°C and 100°C), (3) Show capability of operation at 300- to 400-W/cm for coated (reflective and antireflective at opposite ends) lasers, (4) Provide relevant growth data for fabrication purposes. Furthermore, we explicitly intended to demonstrate that these goals can be achieved in a production environment. On the basis of data presented in the report, the required technology transfer must be judged a complete success.

High-power laser diodes were developed that meet the basic requirements for ranging applications. They are based on the LOC (large optical cavity) heterojunction laser and are optimized to provide fundamental transverse mode operation. This was accomplished by appropriate heterojunction spacing and refractive index steps to prevent the propagation of high-order modes. The devices are designed for cw operation at a power emission of 400 W/cm of emitting facet. With antireflecting films, they can withstand up to 1200 W/cm of instantaneous peak power with a 100-ns pulse and can operate efficiently at temperatures $>75^\circ\text{C}$. This new structure was made possible by the sophisticated liquid-phase epitaxial technology developed at RCA Laboratories, with which large-area wafers of closely controlled dopant composition and layer thickness can be grown. The technology has been successfully transferred to the RCA laser diode manufacturing facility where devices equivalent to those obtained in the laboratory have been produced under model shop conditions. The impact of the devices developed under this program is that high-volume manufacture (with high yields) of structures designed for fusing and other ranging applications will be possible.

UNCLASSIFIED

SECURITY CLASSIFICATION OF THIS PAGE(When Data Entered)

FOREWORD

This Final Report was prepared by RCA Laboratories, Princeton, New Jersey, under Air Force Contract F33615-74-C-1016, *GaAlAs Fuse Development*, Project No. 2001, and Task No. 01. It describes work performed from 1 December 1973 to 30 November 1974 in the Materials Research Laboratory, J. J. Tietjen, Director. The Project Supervisor was H. Kressel and the Project Scientist was H. F. Lockwood. Other members of the Technical Staff at RCA Laboratories who participated in the research are M. Ettenberg and H. S. Sommers. J. Butler contributed to the effort as a consultant while engineering personnel of RCA Electronic Components, located at Lancaster, PA, performed a large part of the diode fabrication and characterization. Technical assistance at RCA Laboratories was provided by: D. Marinelli, V. Cannuli, D. Gilbert, A. Kan, M. Harvey, and I. Hegyi.

The Air Force Project Monitor was Mr. Robert L. Harris, AFAL/TEO.

TABLE OF CONTENTS

Section	Page
I. INTRODUCTION	1
II. MULTIPLE LAYER EPITAXY	3
III. LASER STRUCTURES	8
IV. CONTROL OF RADIATION PATTERNS.	11
A. Symmetrical Structures	11
B. Asymmetrical Waveguide Structures.	17
V. EXPERIMENTAL RESULTS: HIGH-POWER LASERS	23
A. Crystal Growth	23
B. Data	25
C. Reliability.	27
D. Radiation Patterns and Beam Collection Efficiency.	34
VI. CONCLUSIONS.	39
REFERENCES	40

LIST OF ILLUSTRATIONS

Figure	Page
1. Schematic illustration of growth boat. In (a) the saturation of the solutions is completed by the source wafer preceding the substrate wafer whereas in (b) each solution is saturated by its own source wafer	4
2. Photograph of seven-bin boat showing bottom as well as top sources in their initial position	4
3. As-grown wafer showing solution adhering to edges and a network of defects along the leading edge. (The crystal has been cleaved through the defective region.)	5
4. A cleaved wafer with defect-free surface. The absence of growth solution on the surface and its planarity are indicative of highly uniform growth	6
5. Cross section of generalized laser structure used in analysis of transverse modes. The radiative recombination occurs in region 3, while regions 2, 3, and 4 constitute the nominal waveguide	9
6. Experimental and theoretical radiation pattern of "leaky" DH laser with 0.25- μ m cavity. The upper figure shows the near-field and the lower, the far-field intensity distribution. Narrow far-field results from spreading of radiation outside the recombination region	13
7. Structures, far-field patterns, and threshold current densities of 5-layer lasers with different internal placement and composition of heterojunctions.	14
8. Threshold gain curves for four-heterojunction structure of Fig. 7(a) as a function of the displacement of the recombination region from the p-side edge of the waveguide region. Each curve is labeled with a specific mode number; 1 is the fundamental mode.	15
9. Spontaneous spectra for lasers shown in Figs. 7(a) and (c). The short wavelength peak discernible in unit 507N is due to radiation from the GaAs:Ge region. Both spectra are distorted on the high energy side due to internal absorption.	17
10. Far-field pattern of asymmetric LOC structure operating in fundamental mode.	18
11. Far-field pattern of a laser diode at 22° and 75°C showing the effect of a narrowing of the far-field pattern due to a change in the refractive index with increasing temperature	19

LIST OF ILLUSTRATIONS (Continued)

Figure	Page
12. (a) Change of the threshold current density with temperature of laser with temperature-dependent radiation pattern change (curve A), compared with laser having temperature-independent radiation pattern (curve B). (b) Angular divergence, θ , at half-power point corresponding to laser of curve A.	20
13. Comparison of electrical and optical pulse through laser L-170 in which the degree of radiation confinement decreased with increasing temperature. The diode current was adjusted to give a constant 3 W of output.	22
14. Schematic illustration of LOC laser developed for high-power and high-temperature operation. Typical parameters are $d_1 = 5$ to $8 \mu\text{m}$, $d_2 = d_3 = d_4 = d_5 = 1 \mu\text{m}$, $d_6 \approx 15 \mu\text{m}$; $x = 0.15$, $y = 0.07$, $z = 0.015$	23
15. Instantaneous or catastrophic facet damage with pulse width increasing from 50 ns (a) to 2 μs (f). The photomicrographs (780X) of the facets show the line of damage in the optical cavity.	29
16. Dependence of facet damage on pulse width for uncoated lasers. The data points for P-630 LOC type lasers are given for coated and uncoated structures and correspond closely to previously obtained data for single-heterojunction lasers (upper curve). The lower curve is data taken on four-heterojunction lasers	33
17. Facet damage observed on high-power LOC laser at the 1200-W/cm operating level. (Facet originally coated with SiO which was removed to obtain this photograph.)	34
18. Far-field radiation pattern of narrow-beam LOC laser.	35
19. Received power vs. conical collecting angle	36
20. Far-field radiation patterns (perpendicular to junction plane) of two essentially identical laser diodes, both having half-power beam widths of 28° . Diode A was grown at RCA Lancaster and passes 75% of emitted radiation through f/1.3 optics (42°). Diode B was grown at RCA Laboratories and passes 65% of emitted radiation through f/1.3 optics.	38

SECTION I

INTRODUCTION

Heterojunction laser diodes of GaAs and (AlGa)As have become increasingly sophisticated structures fabricated by liquid-phase epitaxy (LPE). Because of progress made both in the technology and in our theoretical understanding of laser diodes, it is now possible to design devices for specific applications. There is general interest in devices both for high peak power (pulsed) operation at room temperature and in diodes capable of reliable continuous room-temperature operation. Both types of devices require low thermal and electrical resistance but other requirements differ. The high-power pulsed lasers need not have very low threshold current densities, but they must be capable of withstanding catastrophic degradation resulting from excessive optical flux density at the emitting facet. The cw lasers, on the other hand, operate at low power levels (tens of milliwatts) and require low threshold current densities to minimize thermal dissipation problems. The beam divergence should be as low as possible in all devices to reduce the size of the external optical collimating system.

In this final report, we discuss techniques used to achieve the control of material parameters of state-of-the-art high-power laser diodes with particular emphasis on the question of radiation pattern control. This subject has come under increasing study in the recent past as models have improved and the technology has been developed, making comparisons between experiment and theory possible. We outline below the primary technical goals of this contract. In addition to the technical goals, it is the explicit intention of this work to demonstrate that the technical goals embodied in the laser diode can be achieved in a production environment, e.g., RCA's Lancaster facility.* On the basis of data to be presented later in this report, the required technology transfer must be judged a complete success.

The primary technical goals of our work are:

- (1) Optimize structure for fundamental transverse mode operation with beam width (FWHM) of approximately $25^\circ - 30^\circ$.
- (2) Demonstrate efficient operation at elevated temperature, i.e., 75°C and 100°C .

*RCA Industrial Tube Division, Lancaster, Pa., 17604.

- (3) Show capability of operation in the 300- to 400-W/cm (0.75 to 1 W/mil) power range for coated (reflective and antireflective at opposite ends) lasers.
- (4) Provide all relevant growth data for production purposes. This will include solution compositions, growth schedule, furnace profile, etc.

SECTION II

MULTIPLE LAYER EPITAXY

As is well known, epitaxial growth of AlAs-GaAs alloys is greatly simplified by the almost perfect match in lattice parameter between these two compounds. The special task of multiple layer growth of laser structures involves growing adjacent layers with widely varying compositions and dopings. The interfaces between these layers must be extremely flat and well defined; there must be no contamination from one growth solution to the next; the layer thickness must be precisely controlled with submicron tolerances; and the final surface must be free of any solution when the wafer is withdrawn from the growing apparatus.

There are many possible designs of the growth apparatus, but the linear (as opposed to circular) multiple bin graphite boat [1] has proven the most popular. Two of many possible designs [2] are shown schematically in Fig. 1. In Fig. 1(a), a GaAs source wafer, usually polycrystalline, precedes the substrate wafer into each bin and assures saturation of the solution before growth on the substrate is initiated. Figure 1(b) is an improvement over this design in that each solution has its own source wafer, and saturation of the solutions is maintained throughout the entire growth cycle. The source wafers are dropped onto relatively small solutions near the growth temperature and are spread over the entire wafer area by the quartz block weights. The resulting thin (typically ≤ 1 mm) solutions yield epitaxial layers the thickness of which can be calculated directly from the phase diagram [3] because the formation of platelets in the solution is greatly reduced. Typical growth efficiencies, defined as the ratio of the thickness grown to that calculated from the phase diagram, range from 0.1 for 1-cm-thick solutions to > 0.9 for solutions 0.2 mm thick. Still more precise saturation can be obtained by adding a bottom source wafer, as in Fig. 1(a), to the thin solution method of Fig. 1(b). Figure 2 is a photograph of a seven-bin boat (with one side removed) which combines the ideas of Figs. 1(a) and 1(b) and is the boat used in

1. H. Nelson, U.S. Patent No. 3,565,702 (1971).
2. H. F. Lockwood and M. Ettenberg, *J. Crystal Growth* 15, 81 (1972).
3. M. Ilegems and G. L. Pearson, *Proceedings of Second Int. Symposium on GaAs*, The Inst. of Physics and the Phys. Soc. London, 1969, p. 3.

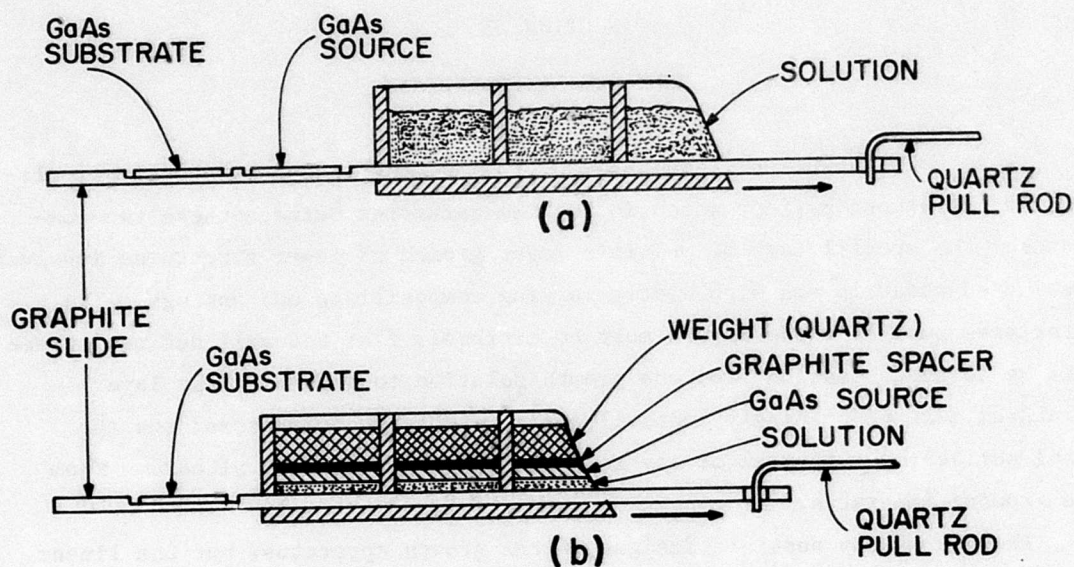


Figure 1. Schematic illustration of growth boat. In (a) the saturation of the solutions is completed by the source wafer preceding the substrate wafer whereas in (b) each solution is saturated by its own source wafer.

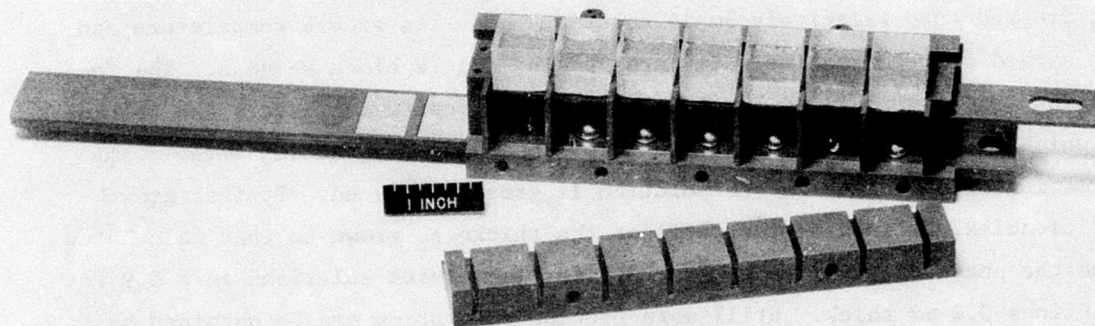


Figure 2. Photograph of seven-bin boat showing bottom as well as top sources in their initial position.

all of the growth runs for this contract. The top sources are shown in their initial position above the 1-gram Ga solutions which will be flattened to 1-mm thickness by the action of the quartz weights.

The reason for this preoccupation with exact melt saturation is apparent if one considers the growth of layers on the order of $0.1\text{-}\mu\text{m}$ thickness. For this same reason, the longitudinal temperature gradient in the growth furnace is also important. If the substrate enters a bin at a temperature higher than the solution in that bin, there may be partial dissolution of the substrate because of undersaturation at the solid-liquid interface; therefore, a decreasing temperature gradient is undesirable when the control of extremely thin layers is involved. An increasing temperature gradient is more favorable because there will be deposition rather than dissolution when the substrate enters a bin which is at a higher temperature. In either case, large temperature gradients require more rapid cooling, thus aggravating the problem of layer thickness control. Typical optimum temperature gradients used for the work reported here are in the range of $0.1^\circ\text{C}/\text{cm}$ along the length of the boat.

The major cause of (liquid) cross-contamination between solutions in adjacent bins is also the cause of poor wiping after the growth of the final epitaxial layer. Any geometric artifact such as a major defect or dendrite on the surface will cause the solution to adhere in that area. Figure 3 is a

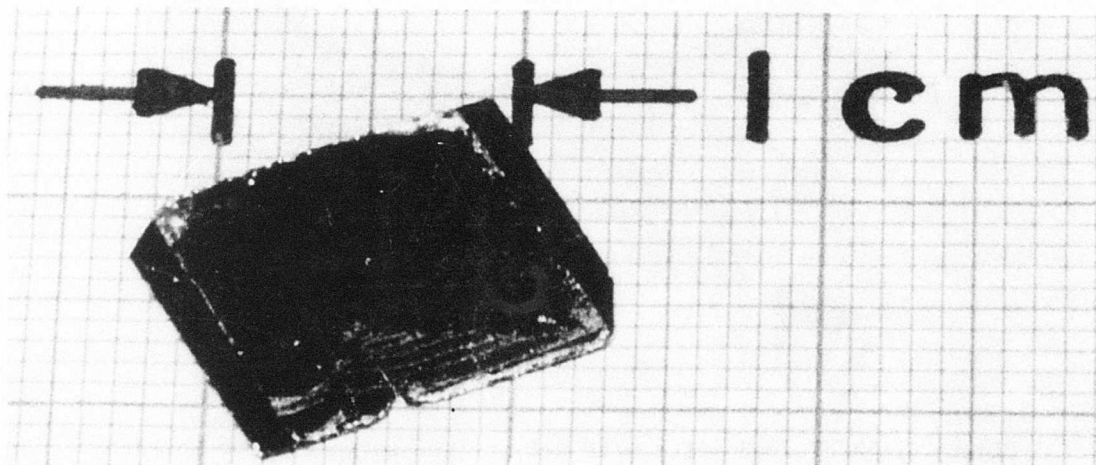


Figure 3. As-grown wafer showing solution adhering to edges and a network of defects along the leading edge. (The crystal has been cleaved through the defective region.)

photograph of the surface of a multiple layer structure which shows some of these effects. Along both sides where the crystal is held in place, dendrites have grown and wiping after the last layer growth is incomplete. Since this inhomogeneity is confined to the edge of the crystal, it is not serious in terms of subsequent processing. However, along the leading edge there is a network of small defects which are made visible by the presence of gallium solution not removed by the final wiping.

Figure 4 is a photograph of multiple layer structure which is free of any surface irregularities. There are gradual steps in this surface with a typical height of only 0.03 to 0.05 μm ; thus, the wafer can be processed for

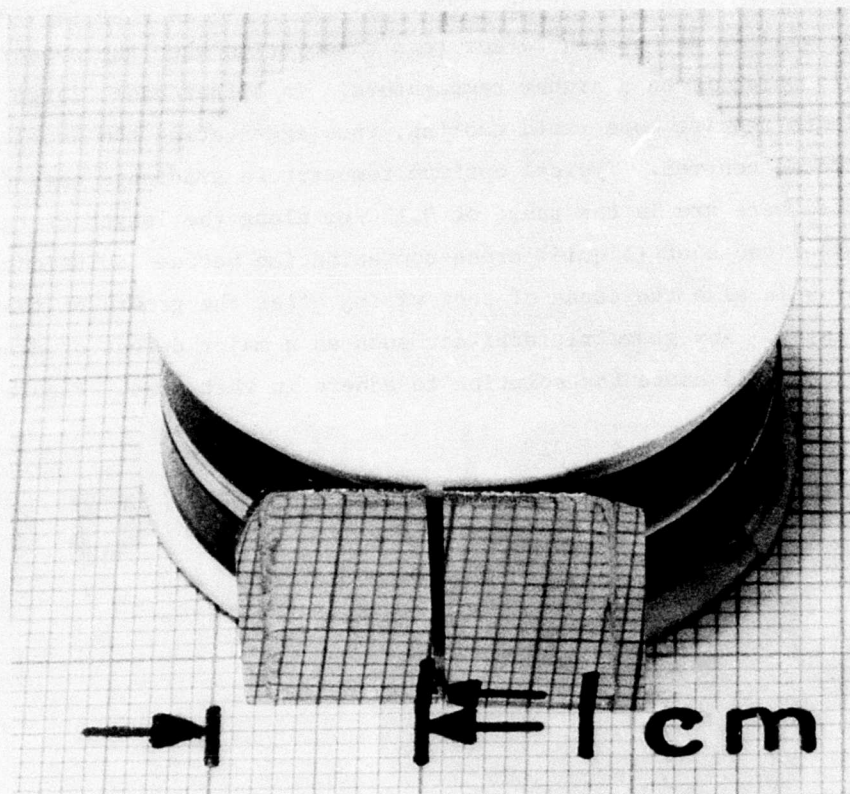


Figure 4. A cleaved wafer with defect-free surface. The absence of growth solution on the surface and its planarity is indicative of highly uniform growth.

ohmic contacting without the need of a polishing step. This is especially important when the active layers of the structure are within a few micrometers of the surface as they are in the cw laser. For the pulsed device (to be described in more detail later in this report), the absence of a polishing step after growth increases the yield and reduces the cost especially in a production environment.

SECTION III

LASER STRUCTURES

Figure 5 is a schematic diagram of a five-layer structure which can be considered the generalized GaAs injection laser [4]. Multiple layer lasers under active study are variations of this structure and contain either some or all of the layers shown. Basically, the laser consists of a radiative recombination region 3 of width d_3 , the "gain region," and a waveguiding region which is either equal to or thicker than the gain region. In Fig. 5 the nominal waveguide region is of thickness $w = d_2 + d_3 + d_4$ with the higher bandgap regions 1 and 5 providing the walls of the waveguide because of their reduced index of refraction at the GaAs lasing photon energy. The difference in the Al content between i-numbered layers determines the refractive index difference Δn which, at the typical 300°K GaAs lasing emission wavelength of $\sim 9000 \text{ \AA}$, increases approximately linearly with the bandgap energy difference ΔE_g . For example, for $\Delta E_g = 0.4 \text{ eV}$, $\Delta n \sim 0.2$ or $\Delta n/n \sim 0.2/3.6 \sim 6\%$ [5]. Carrier confinement requires a potential barrier height of a few kT. At 300°K, a bandgap energy difference of ~ 0.1 is adequate.

Various heterojunction laser structures are obtained by using selected layers in Fig. 5. If $d_2 = d_3 = 0$ and $x(5) = x(1)$, we obtain the symmetrical double heterojunction (DH) laser [6,7]. With $d_2 = 0$ and $x(4) = 0$, the large optical cavity (LOC) laser diode is obtained [8]. A four-heterojunction laser is obtained when all the regions are used [9]. Each of these structures is capable of a wide range of properties depending on the width of the various regions, their Al content, symmetry, and doping in the GaAs recombination region. We will discuss some of these properties later in the report but for identification purposes, a modification of the LOC structure is the device being delivered under the terms of this contract.

4. J. K. Butler, J. Appl. Phys. 42, 4447 (1971).
5. H. Kressel, H. F. Lockwood, and J. K. Butler, J. Appl. Phys. 44, 4095 (1973).
6. Zh. I. Alferov, M. V. Andreev, V. I. Korol'kov, E. L. Portnoi, and D. N. Tretyakov, Sov. Phys.-Semicond. 2, 1289 (1969).
7. I. Hayashi, M. B. Panish, P. W. Foy, and S. Sumski, Appl. Phys. Letters 17, 109 (1970).
8. H. F. Lockwood, H. Kressel, H. S. Sommers, Jr., and F. Z. Hawrylo, Appl. Phys. Letters 17, 499 (1970); H. Kressel, H. F. Lockwood, and F. Z. Hawrylo, J. Appl. Phys. 42, 561 (1972).
9. G. H. B. Thompson and P. A. Kirkby, IEEE J. Appl. Phys. 42, 561 (1972).

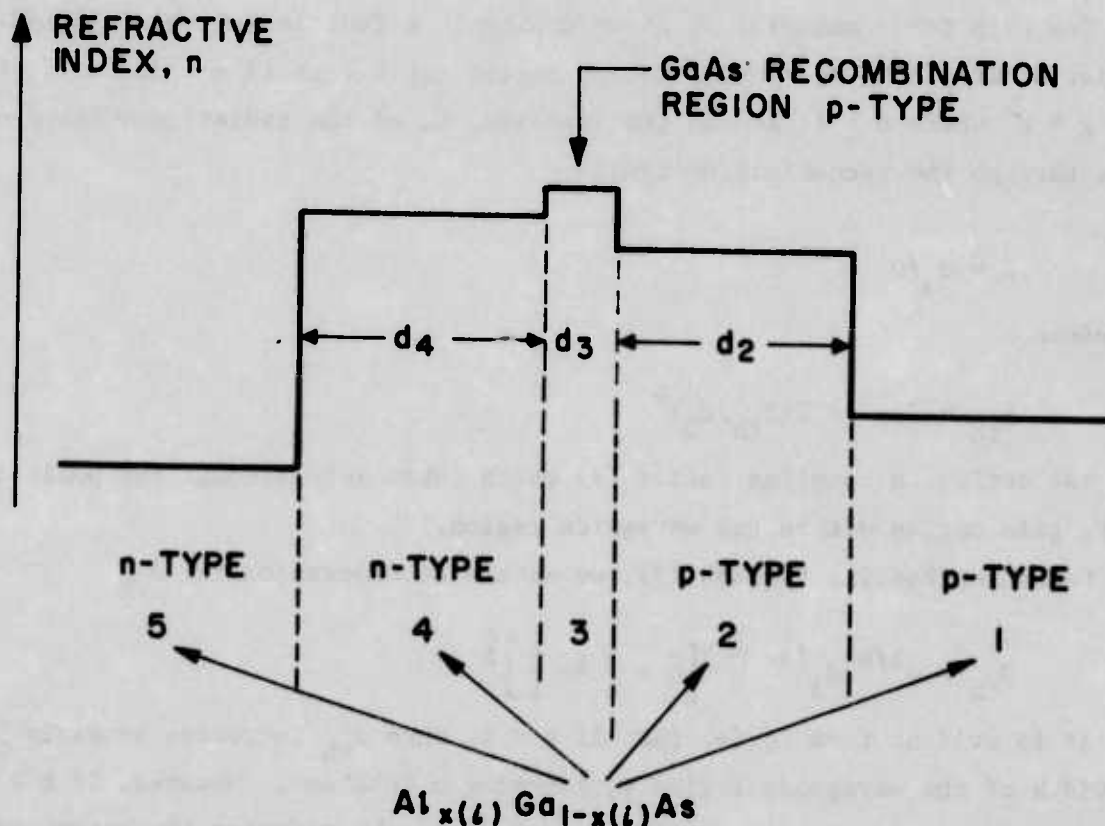


Figure 5. Cross section of generalized laser structure used in analysis of transverse modes. The radiative recombination occurs in region 3, while regions 2, 3 and 4 constitute the nominal waveguide.

The threshold current density of the laser depends on the width of the various regions and on the doping level in the recombination region. This becomes evident from basic considerations which we review below.

At a given temperature, the laser threshold current density J_{th} is a function of the optical waveguide thickness w , the width of the recombination region d_3 , the doping level, the facet reflectivity R , and the length of the laser L . The gain coefficient required to reach threshold, g_{th} , is

$$g_{th} = \bar{\alpha} + \frac{1}{L} \ln \frac{1}{R}, \quad (1)$$

where $\bar{\alpha}$ is the effective absorption coefficient. The major contribution to $\bar{\alpha}$ is due to free carrier absorption in well-designed heterojunction lasers.

The gain for a material of given doping is a function of the injected carrier density n in the recombination region (at threshold $n \propto J_{th}/d_3$), of the form $g \propto n^b$ where $b \geq 1$, and of the fraction, Γ , of the radiation which propagates through the recombination region

$$\Gamma \approx d_3/w \quad (2)$$

Therefore,

$$g_{th} \propto \Gamma n^b \propto \Gamma (J_{th}/d_3)^b. \quad (3)$$

(We neglect a coupling factor [9] which takes into account the position of the gain region within the waveguide region.)

Combining Eqs.(1) through (3), we obtain an expression for J_{th}

$$J_{th} \propto w^{1/b} d_3^{(1-\frac{1}{b})} \left[\bar{\alpha} + \frac{1}{L} \ln \frac{1}{R} \right]^{\frac{1}{b}} \quad (4)$$

It is evident from Eq.(4) that if $b = 1$, then J_{th} increases linearly with the width of the waveguide region w , assuming $\bar{\alpha}$ constant. However, if $b > 1$, then for constant w , it is possible to reduce J_{th} by reducing the recombination region width d_3 . Dependent upon the doping, LOC devices exhibit a value of b between 1 and 2.

SECTION IV

CONTROL OF RADIATION PATTERNS

In view of the problem of collimating the output of semiconductor laser diodes, it is of technological interest to obtain diodes with as narrow a beam as possible. Simply increasing the thickness of the mode-guiding region of the device does not assure reduced divergence of the transverse beam because high-order transverse modes are usually favored which give rise to a "rabbit-ear" pattern with angular separations which depend on the details of the structure. The subject of beam control has received increasing attention as the liquid-phase technology has advanced, allowing improved control of layer thickness and composition. In this section we will consider some major results which illustrate the type of devices now possible using symmetrical and asymmetrical structures.

Information concerning the order of the dominant transverse mode can be deduced from near-field measurements, but more reliably, from an accurate determination of the far-field radiation pattern perpendicular to the plane of the junction. The order of the mode producing the far-field radiation pattern can usually be deduced from the number of lobes. The fundamental mode, $m = 1$, gives rise to a single lobe while higher-order modes give rise to additional lobes; the mode number for $m > 1$ is given by

$$m = 2 + (\text{number of low-intensity lobes between the two major lobes}). \quad (5)$$

Other useful data are the angular separation between the two large lobes and the angular beamwidth of each lobe. The angular separation between the lobes depends on the value of Δn at the heterojunctions while the lobe width is related to the width of the mode-guiding region [10].

A. SYMMETRICAL STRUCTURES

While the threshold current density of a DH laser is decreased by reducing the heterojunction spacing, this decrease is typically accompanied by a broadening of the radiation pattern (in the direction perpendicular to the junction) to half-power angular values as high as $\sim 80^\circ$.

10. J. K. Butler and H. Kressel, J. Appl. Phys. 43, 3402 (1973).

The simplest way of decreasing the DH beam divergence without excessive increase in the threshold current density is to allow a controlled degree of radiation spread outside of a very narrow recombination region [11]. As long as the waveguide formed is symmetric in its refractive index discontinuity, mode-guiding is possible even if only a fraction of the radiation is confined to the recombination region. Figure 6 shows the near-field optical intensity and far-field pattern of such a "leaky" DH laser which compares closely with the theoretically calculated radiation pattern. Lasers with this type of construction have been made with threshold current densities of about 1400 A/cm^2 and with half-intensity beam angular separations of 20 to 25° . It is clear that tight control of the Al concentration and heterojunction spacing is needed to obtain reproducibly a desirable combination of radiation pattern and threshold current density.

The addition of two outer heterojunctions [regions 2 and 4 in Fig. 5] makes it easier to reproduce a narrow beam because these prevent excessive radiation spread. The effect of the placement of the heterojunctions and of the recombination region on the radiation patterns can be illustrated with a series of experimental devices [12]. Figure 7(a) shows the dimensions of a four-heterojunction diode structure with a GaAs:Si recombination region $0.5 \mu\text{m}$ thick. The adjacent regions 2 and 4 consist of $\text{Al}_{0.03}\text{Ga}_{0.97}\text{As}$, while regions 1 and 5 consist of $\text{Al}_{0.15}\text{Ga}_{0.85}\text{As}$. The separation between the outer heterojunctions is $3.7 \mu\text{m}$. The radiation pattern of this laser operating in the fundamental mode is shown on the left side of Fig. 7(a). It consists of a single lobe in the direction perpendicular to the junction with a beam divergence of 17° at the half-power point, which corresponds to the diffraction limit of a $3\text{-}\mu\text{m}$ aperture. Both the inner and outer sets of heterojunction contribute to the radiation confinement, with the inner ones tending to peak the field in the recombination region and thus promoting fundamental transverse mode operation.

A theoretical analysis [13] of the gain for the various transverse modes of a four-heterojunction laser of the type shown in Fig. 7(a) is presented in Fig. 8. This shows clearly that the fundamental mode is preferred since its

11. H. Kressel, J. K. Butler, F. Z. Hawrylo, H. F. Lockwood, and M. Ettenberg, RCA Review 32, 393 (1971).
12. Some of these results were presented by the authors at the IEEE Device Research Conference, Boulder, Colorado, June 1973.
13. J. K. Butler, private communication, 1973.

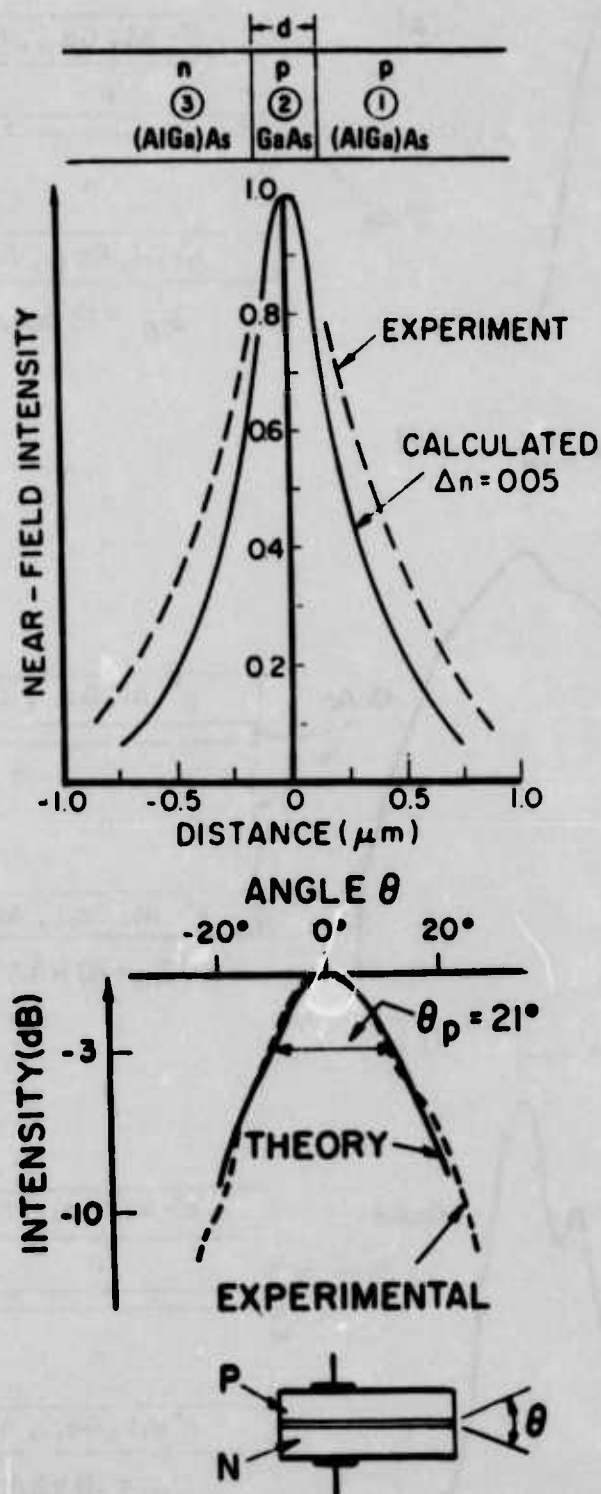


Figure 6. Experimental and theoretical radiation pattern of "leaky" DH laser with 0.25- μm cavity. The upper figure shows the near-field and the lower, the far-field intensity distribution. Narrow far-field results from spreading of radiation outside the recombination region.

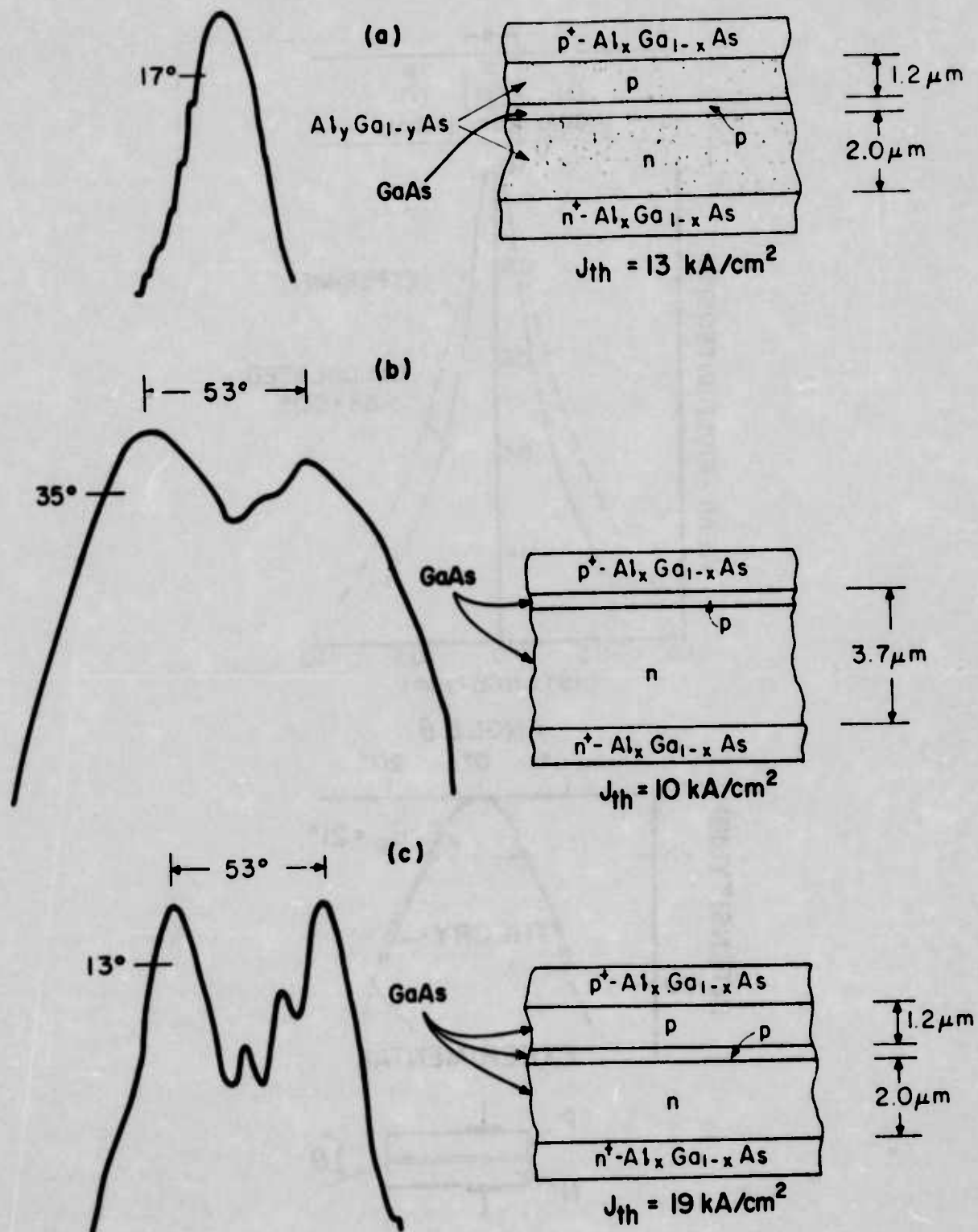


Figure 7. Structures, far-field patterns, and threshold current densities of 5-layer lasers with different internal placement and composition of heterojunctions.

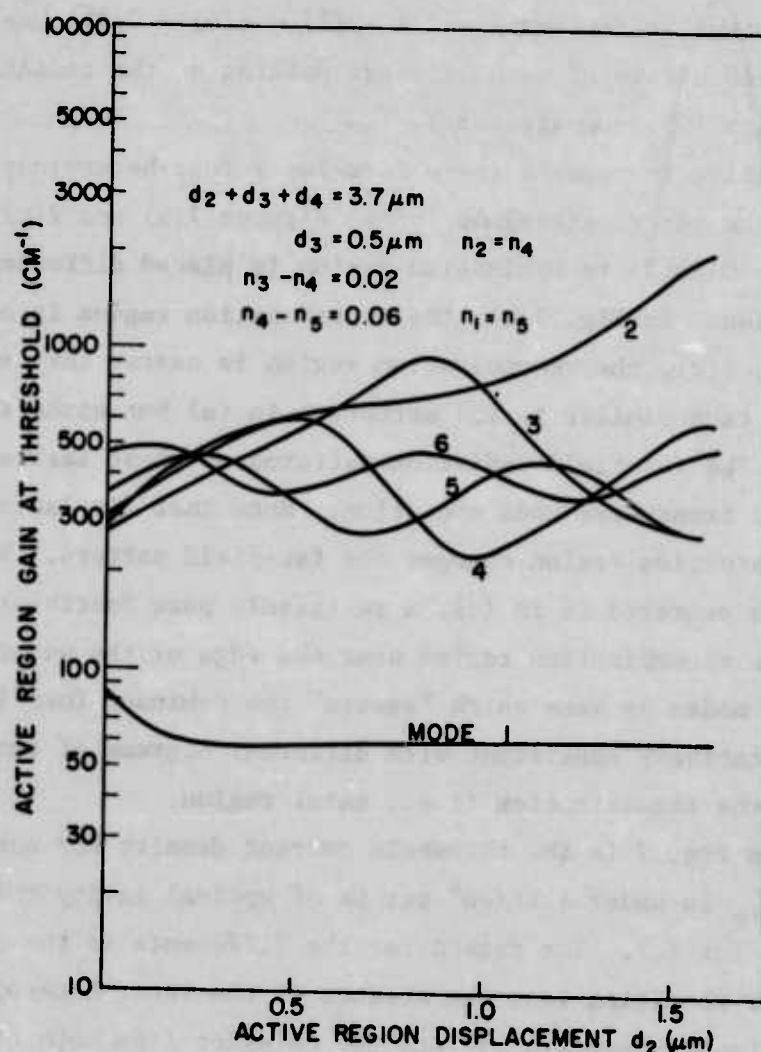


Figure 8. Threshold gain curves for four-heterojunction structure of Fig. 7(a) as a function of the displacement of the recombination region from the p-side edge of the waveguide region. Each curve is labeled with a specific mode number; 1 is the fundamental mode.

gain coefficient in this particular structure is much lower than the gain for the other modes. Furthermore, the position of the recombination region within the waveguide region is not critical. This prediction has been experimentally confirmed. For example, we found that structures, similar except that the recombination region was placed either $1.2 \mu\text{m}$ or $2.5 \mu\text{m}$ from the p-p interface, had radiation patterns identical to those of the structure shown in Fig. 7(a). The radiation pattern is sensitive, however, to the barrier height of the inner heterojunctions. For example, a structure similar to that discussed above but

with higher Al content in regions 2 and 4 [$x(2) = x(4) = 0.06$] has a beam divergence of 35° , indicative of much stronger peaking of the radiation near the recombination region ($\sim 1.5\text{-}\mu\text{m}$ aperture).

It is instructive to compare these five-layer four-heterojunction structures with and without the inner heterojunctions. Figures 7(b) and 7(c) show two examples where the GaAs:Si recombination region is placed differently within the waveguide region. In Fig. 7(b), the recombination region is near the p^+-p interface; in Fig. 7(c), the recombination region is nearer the center of the waveguide region, thus similar to the structure in (a) but without the inner heterojunctions. The far-field radiation patterns of these lasers are indicative of high-order transverse mode operation. Note that displacing the position of the recombination region changes the far-field pattern. With the recombination region centered as in (c), a relatively pure fourth-order mode is seen, but with the recombination region near the edge of the waveguide as in (b), a mixture of modes is seen which "smears" the dominant four lobes. This behavior is qualitatively consistent with different degrees of coupling of the radiation to the recombination (i.e., gain) region.

Also shown in Fig. 7 is the threshold current density for each structure. In (a) and (b), J_{th} is under 4 kA/cm^2 per μm of optical cavity thickness, but it is much higher for (c). The reason for the difference is the poor carrier confinement in (c) resulting from the absence of the inner heterojunctions. In fact, the spontaneous spectra reflect the emission from both the GaAs:Si and the GaAs:Ge region in (c) as can be seen in Fig. 9. The lasing occurs in the GaAs:Si region, and thus the carriers diffusing beyond that region are wasted, resulting in a relatively high threshold current density.

In the above examples the recombination region is relatively thin. It has also been shown experimentally that fundamental mode operation can be promoted in a LOC structure by making the recombination region occupy a significant portion of the total waveguide region [14]. In this way, the gain coefficient of the fundamental mode is increased by improving its coupling to the gain region. However, in order to minimize the absorption, it is essential that the recombination region be still smaller than the minority-carrier diffusion length.

14. T. L. Paoli, B. W. Hakki, and B. I. Miller, J. Appl. Phys. 44, 1276 (1973).

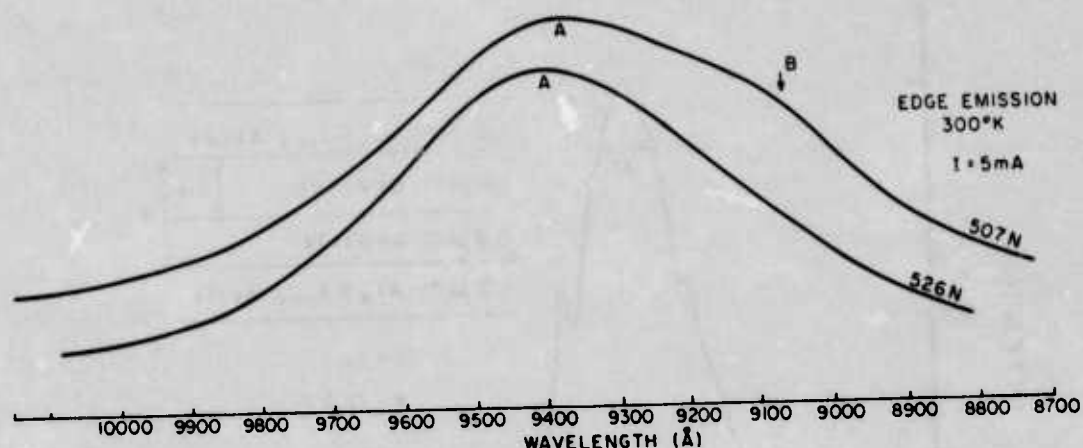


Figure 9. Spontaneous spectra for lasers shown in Figs. 7(a) and (c). The short wavelength peak discernible in unit 507N is due to radiation from the GaAs:Ge region. Both spectra are distorted on the high energy side due to internal absorption.

B. ASYMMETRICAL WAVEGUIDE STRUCTURES

We now turn our attention to mode control in asymmetrical dielectric structures. It is well known that guided wave propagation is impossible below a critical value of the waveguide thickness for a given asymmetry and minimum refractive index difference at one boundary.

The theory of asymmetrical waveguides as applied to laser diodes of the LOC type has been extensively described [10]. Briefly, the propagation of the highest transverse mode order allowed depends on the dielectric asymmetry, the waveguide thickness, the lowest refractive index step value on one side of the waveguide, and the relative recombination region width. By choosing structures with sufficiently small index values, it is possible to limit the operation to the fundamental mode only. Figure 10 shows an example of an asymmetrical LOC unit operating in the fundamental mode with a 14° beam. This is accomplished by allowing the radiation to leak out of the $1.8\text{-}\mu\text{m}$ -wide waveguide region into the n-type (AlGa)As.

Asymmetrical structures are also interesting because under certain conditions it is possible to observe dramatic changes in the degree of radiation confinement resulting from a reduction of the refractive index difference at the n-n barrier with increasing temperature. An example of the increase in

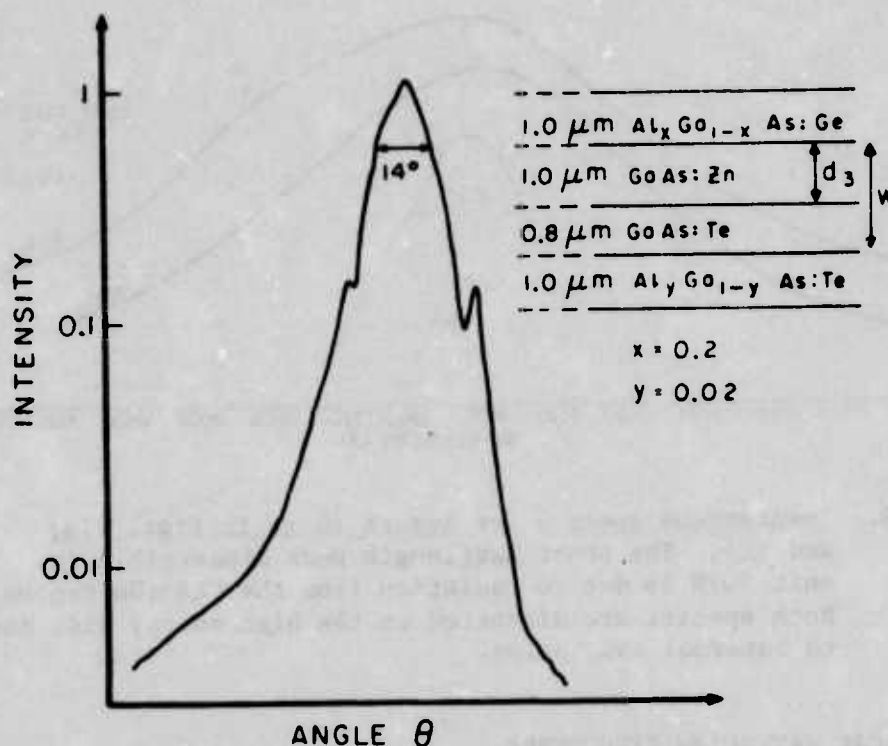


Figure 10. Far-field pattern of asymmetric LOC structure operating in fundamental mode.

the radiation spread with temperature in one diode is illustrated in Fig. 11, which shows at 22°C a $\theta = 20^\circ$ beam, while at 75°C, θ is reduced to 10° . This beam reduction results from an effective aperture doubling due to leakage of radiation, mainly into the (AlGa)As n-type region. Another perspective on the effect of this increased leakage is obtained from the data shown in Fig. 12. The threshold current density of such a structure increases steeply with temperature [Fig. 12(a)] as the radiation confinement is decreased, Fig. 12(b). For comparison we also show the J_{th} dependence on temperatures due to higher heterojunction barriers. In such a strongly confined unit (with θ constant) the threshold current density only doubles between 22° and 70°C, while in the "leaky" asymmetrical unit it increases by a factor of ~ 10 .

The index discontinuity at the n-n barrier in the device of Fig. 11 was created by the incorporation of small (typically $< 3\%$) amounts of Al in the n-type dielectric wall of the cavity. The single-heterojunction laser achieves similar index discontinuities by heavy compensation in the recombination region

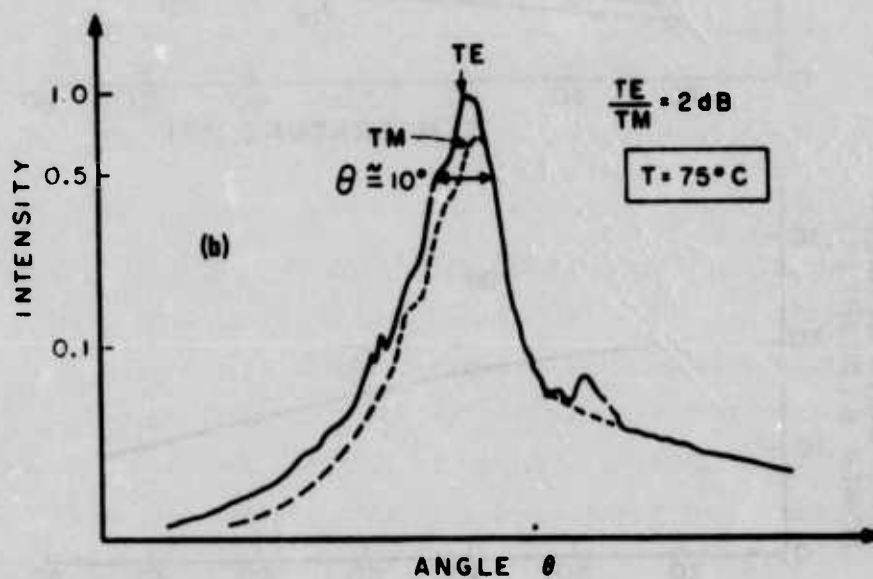
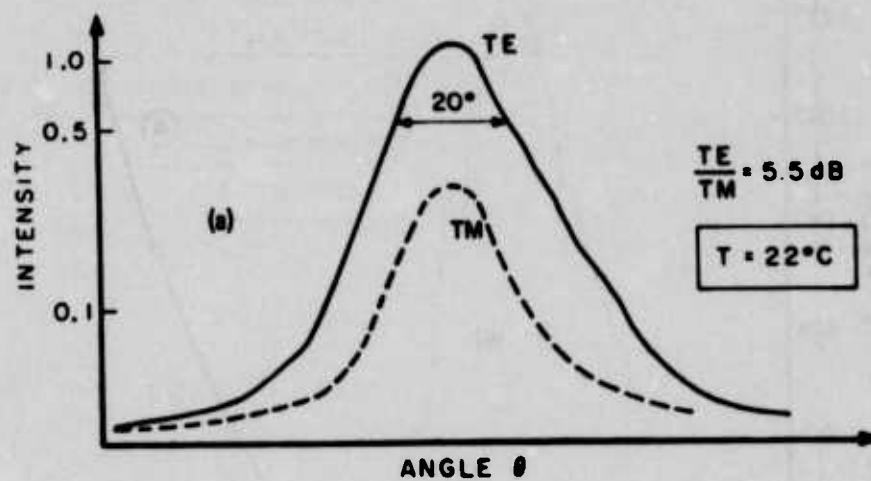


Figure 11. Far-field pattern of a laser diode at 22° and 75°C showing the effect of a narrowing of the far-field pattern due to a change in the refractive index with increasing temperature.

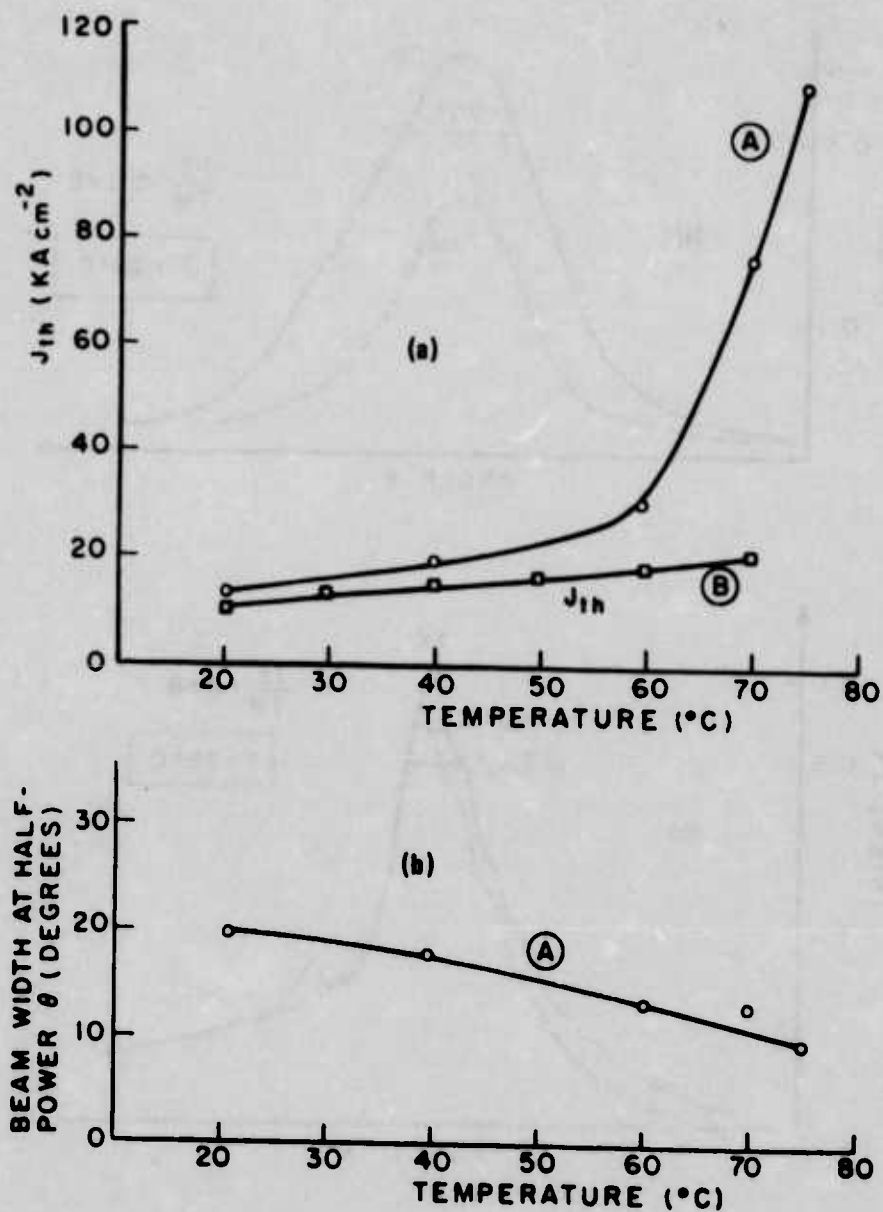
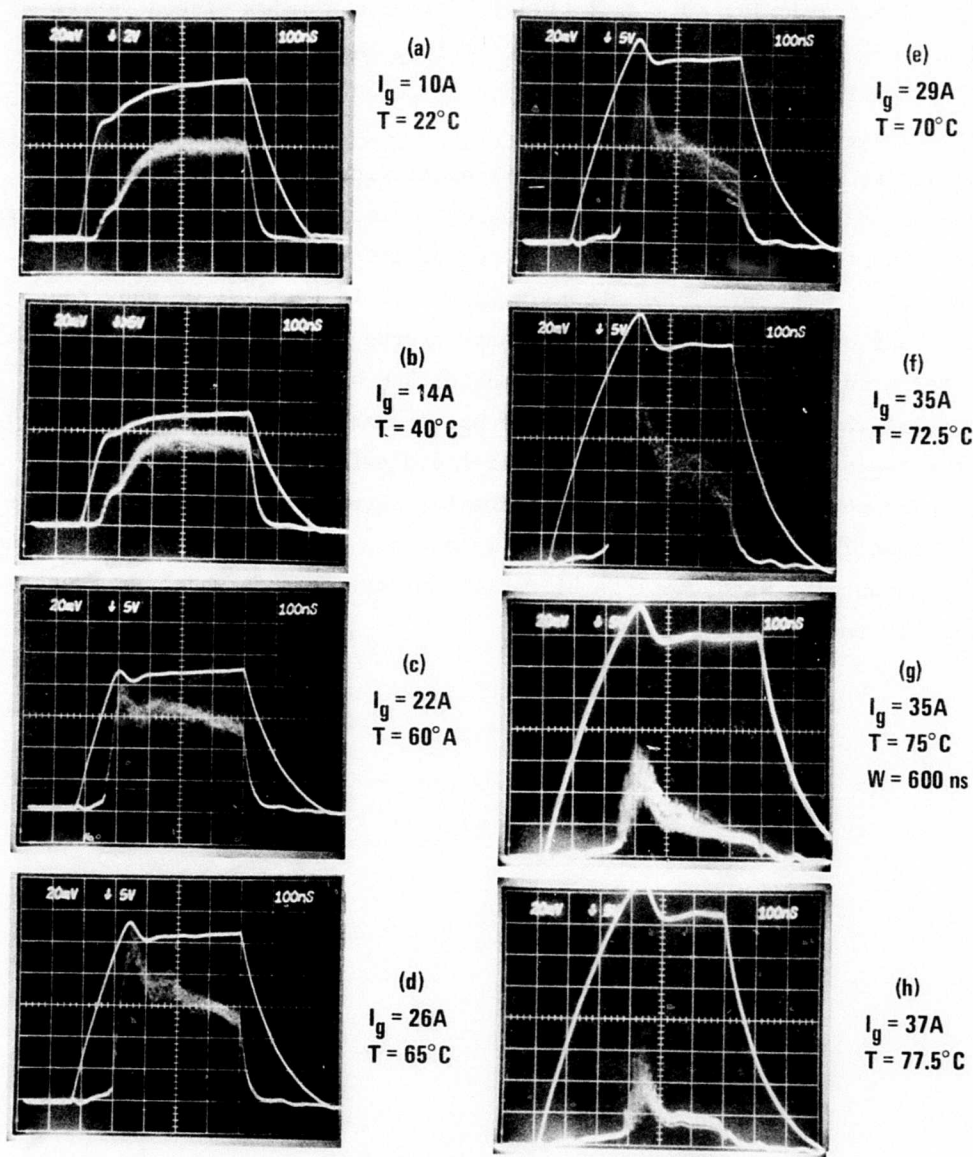


Figure 12. (a) Change of the threshold current density with temperature of laser with temperature-dependent radiation pattern change (curve A), compared with laser having temperature-independent radiation pattern (curve B). (b) Angular divergence, θ , at half-power point corresponding to laser of curve A.

(p-type) and heavy doping outside (n-type). Since the index discontinuity created by doping is quite temperature-sensitive, the performance of single-heterojunction lasers is intrinsically more temperature-sensitive than that of multiple-heterojunction devices.

The strong reduction in optical confinement with increasing temperature also affects the shape of the radiated optical pulse for a given current pulse. One finds that the optical pulse shape deteriorates markedly with evidence of instability in the output as shown in Fig. 13. In Fig. 13, we show the electrical and optical pulse shape for temperatures between 22° and 75°C, the current being adjusted in each case to provide 3 W of output. Note that the optical pulse shape deterioration becomes particularly noticeable at 65°C and above, the temperature range where the far-field pattern most noticeably narrows. The above optical pulse anomalies have been seen before in single-heterojunction lasers, and both in those lasers and the present one, the effect is clearly connected with the loss of radiation confinement, which apparently gives rise to unstable cavity modes.



#2 LOC-170P, Curr. Pulse: Per. = 100 Hz
 $P_{out} = 10 mW/mV$, $W = 500 ns$ [except (g)],

Figure 13. Comparison of electrical and optical pulse through laser L-170 in which the degree of radiation confinement decreased with increasing temperature. The diode current was adjusted to give a constant 3 W of output.

SECTION V

EXPERIMENTAL RESULTS: HIGH-POWER LASERS

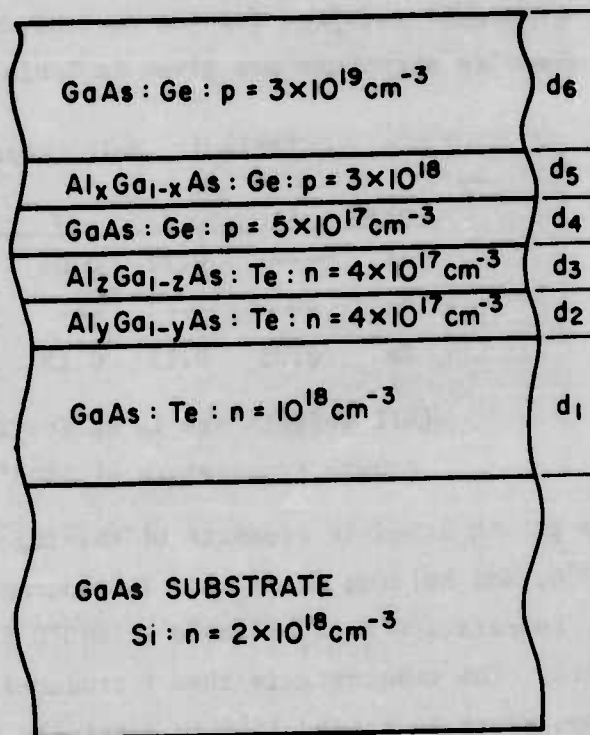
In this section we tabulate the detailed results of the growth runs made both at RCA Lancaster and RCA Princeton. Consistent with the terms of the contract, five growth runs were predesignated in each location expressly for final delivery of devices. That is, no selection of five runs from a larger number was made.

From each run, slivers were chosen randomly after processing, and from these slivers 10 diodes were mounted on packages. Of these 10 diodes, five were chosen for delivery, and two of the five were fully characterized with respect to threshold current density, efficiency, temperature behavior, and beam pattern. Later in this section we will comment about operating life.

A. CRYSTAL GROWTH

All of the growth runs were made using the thin-solution method outlined in Section II. Each wafer had a total of six epitaxial layers. The structure is shown in Fig. 14. The first layer grown on the substrate is n-type GaAs,

Figure 14.
Schematic illustration of LOC laser developed for high-power and high-temperature operation. Typical parameters are $d_1 = 5$ to $8 \mu\text{m}$, $d_2 = d_3 = d_4 = d_5 = 1 \mu\text{m}$, $d_6 \approx 15 \mu\text{m}$; $x = 0.15$, $y = 0.07$, $z = 0.015$.



which serves as a new substrate for the subsequent layer growth. We have found this layer indispensable in the control of subsequent layer thickness, uniformity, and perfection; it is nominally 5 to 8 μm thick.

The optical cavity is located between layers 2 and 5, and since the radiation is rather well confined, thickness of these layers is not critical. Their nominal thickness is 1 μm each. The heavily doped "cap" layer of GaAs:Ge is also not critical in thickness for the present application, and for production ease d_6 is generally about 15 μm . For very high-duty-factor operation, this layer is made as thin as 1 μm .

The cavity itself, layers 3 and 4, has critical dimensions in terms of beam control. To assure fundamental transverse mode operation, $d_3 + d_4$ is kept at $2 \pm 0.1 \mu\text{m}$ with the p-n junction placed approximately ($\pm 0.2 \mu\text{m}$) in the middle. In addition, the value of z in $\text{Al}_z\text{Ga}_{1-z}\text{As}$ is kept at $z = 0.015$ to give a beam width (FWHM) of approximately 30° . If $z = 0$, the device will revert to the next higher transverse mode with a double-lobed beam requiring larger numerical aperture optics for efficient collection. The Al concentrations in the guiding layers are given by $x = 0.15$ and $y = 0.07$. The beam can be made considerably narrower than 25 to 30° by adjusting z and y (see Fig. 12), but there is a price to pay in threshold current, especially at the higher temperatures required for the current work. The exact melt compositions for the entire structure are given in Table 1.

Table 1. Melt Compositions

Layer	1	2	3	4	5	6
Al	---	0.22	0.05	---	0.5	---
Ge	---	---	---	5.0	50	100
Te	0.35	0.15	0.15	---	---	---

(All weights are in mg for 1-g Ga melts at a growth temperature of $\sim 800^\circ\text{C}$.)

The growth schedule consists of raising the temperature to 850°C , cooling to 800°C , and holding for 1 hr. The source wafers are then dropped, after which the temperature is again held at 800°C for 1 hr to assure saturation of the melts. The substrate is then introduced into the first solution, and the temperature is raised 15°C to partially dissolve the substrate. Growth of the

first layer starts at 815°C and ends at 800°C at which time the substrate enters the second bin. This process is repeated for all the subsequent layers at a continuous cooling rate of 0.5°C/min. The temperature changes (in °C) necessary to grow each layer are: $\Delta T_1 = 15$, $\Delta T_2 = 2.3$, $\Delta T_3 = 1.54$, $\Delta T_5 = 3.1$, $\Delta T_6 = 30$.

B. DATA

Table 2 lists the relevant physical measurements of the lasers to be delivered. The lasing wavelength at 23°C is $8900 \pm 50 \text{ \AA}$; at 75°C, it is $9050 \pm 50 \text{ \AA}$. Threshold current densities (J_{th}) and differential quantum efficiencies (η) were measured with the aid of a calibrated ITT-4000 photodiode, with the lasers driven by a 200-ns current pulse. The output of the lasers is single-ended; i.e., there is a reflective coating on the rear and a near anti-reflective coating (SiO) on the front facet. The reflective coatings on runs L-192 and P-638 were defective for the particular diodes randomly chosen, and this explains their poor performance. Thus, radiation is emitted strongly from the rear of these diodes and the far-field pattern is distorted by reflections from the header. Naturally, the efficiency is also reduced because this scattered light is not collected by the detector.

The variability in performance seen in Table 2, although not excessive, does not truly represent the far greater uniformity inherent in the epitaxial process itself. The two most important contributions to scatter in the data are precise control of elemental Al in the melt and control of the optical thickness (index of refraction x actual thickness) of the antireflective coating. Both of these problems were essentially solved during the last weeks of the contract period and are not reflected in the data of Table 2.

From the compositions shown in Table 1, it is clear that extremely small concentrations of Al are required in the melts. This is particularly true of layer 3, the layer having the most profound effect upon the far-field radiation pattern. Two factors influence the accuracy of the Al incorporated into the $Al_zGa_{1-z}As$: (1) oxygen contamination with the subsequent formation of Al_2O_3 , and (2) operator error in handling microgram quantities of substances, a factor eliminated by appropriate training. By redesigning the input (H_2) gas flow system, oxygen contamination has been reduced considerably below

Table 2. Relevant Parameters of Delivered Lasers

Run (a)	$J_{th}(23^{\circ}C)$ kA/cm ²	η %	$J_{th}(75^{\circ}C)$ kA/cm ²	η %	θ_{\perp} deg	$\theta_{ }$ deg
L-175-1	11.9	52	24.6	32	32	14
L-175-2	11.9	52	23.5	32	32	16
L-176-1	8.64	52	16.3	41	32	15
L-176-2	8.47	52	15.8	41	32	15
L-188-1	9.8	50	17.3	44	23	13
L-188-2	9.6	50	16.6	44	23	12
L-190-1	9.6	53	15.4	37	31	19
L-190-2	9.8	53	16.6	34	37	18
L-192-1	9.5	14	20.8	12	30	(b)
L-192-2	9.6	20	19.2	16	35	(b)
P-630-1	8.9	43	18	32	30	12
P-630-2	10	50	19	32	27	12
P-634-1	11.9	57	25.8	35	28	14
P-634-2	11.7	49	23.5	36	28	13
P-635-1	10.5	50	19.8	34	29	14
P-635-2	10.9	53	20.7	41	26	14
P-636-1	12.4	47	25.8	44	25	16
P-636-2	12.6	57	24.5	35	28	14
P-638-1	13.7	19	17	15	29	(b)
P-638-2	12.3	7	18	10	32	(b)

NOTES:

- (a) Prefix L or P refers to RCA Lancaster or RCA Princeton material, respectively.
- (b) See text for discussion.
- (c) Lasing wavelength: $\lambda_L(23^{\circ}C) = 8900 \pm 50 \text{ \AA}$; $\lambda_L(75^{\circ}C) = 9050 \pm 50 \text{ \AA}$.
- (d) $J_{th}(100^{\circ}C) = 25$ to 35 kA/cm^2 for all lasers.

1 ppm. The removal of oxygen also noticeably improves the crystal quality and permits defect-free growth; see Fig. 4 for an example of a defect-free surface.

Variations in the optical thickness of the antireflective coating account for most of the run-to-run variations in threshold current density. For a given run, the typical variation in threshold current density from lasers taken from the entire wafer is less than 10%, with a somewhat larger variation in the external quantum efficiency.

C. RELIABILITY

The major reliability question that arises for high-power lasers is one of facet damage rather than bulk degradation. That is, given high-quality defect-free crystal growth and good control over impurities, lasers which are operated at high power levels inevitably fail mechanically at the facet and not through the generation of bulk defects which might lower the internal quantum efficiency.

We have performed experiments to determine (1) the mechanical factors affecting the onset of facet damage, (2) pulse duration dependence of facet damage, and (3) the specific damage threshold of those diodes delivered under the present program.

It has been established over the years that facet damage is associated with peak optical intensity. Many mechanisms, including stimulated Brillouin scattering, piezoelectric-induced strain, and electrostriction, have been invoked to explain surface damage, but definitive experiments to isolate the cause have not been devised.

We have discovered that there are preferred nucleation sites for catastrophic damage. These sites are inevitably mechanical in nature. For instance, in relatively narrow (100 μm) lasers with apparently perfect facets, damage frequently initiates at the edge of the laser where it has been wire-sawed. The resulting surface disturbance appears to occupy an area less than 1 μm x 1 μm , but this region serves as the lowest threshold nucleation site for additional damage. As a result, a line of damage travels across the laser facet and destroys the mirror of the Fabry-Perot cavity and reduces the optical output. Occasionally the damage stops before destroying the entire facet,

and the diode continues to lase at a lower efficiency. This cessation of damage may be related to the lateral homogeneity of the optical field in the cavity at the surface.

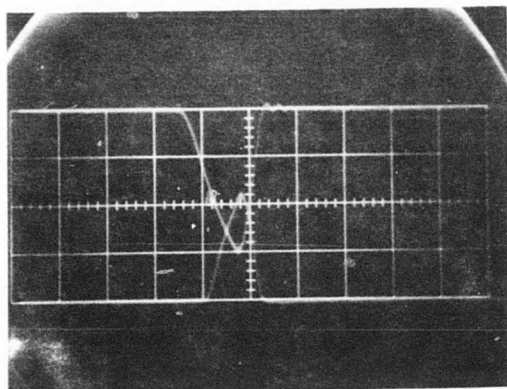
If the sawed edges are physically removed from the lasing region, which is the case for the stripe geometry, there is a dramatic improvement in the threshold for catastrophic damage. When damage does occur, it will start at any scratch crossing the optical cavity and radiate in both directions.

If the surface is free of scratches (in the sense of not being visible at 2000X magnification with differential phase contrast), there is a further increase in the threshold for damage. The next surface feature for damage nucleation is the cleavage striation. This surface defect appears to be present to a greater or lesser extent in all diodes, and the more obvious the striation, the lower the damage threshold.

These effects are not small. Scratched diodes have been found to damage at one-sixth the optical power of similar unscratched diodes in a stripe configuration. Diodes with cavities defined by sawed edges tend to damage at powers one-half to one-third that of stripe-geometry diodes.

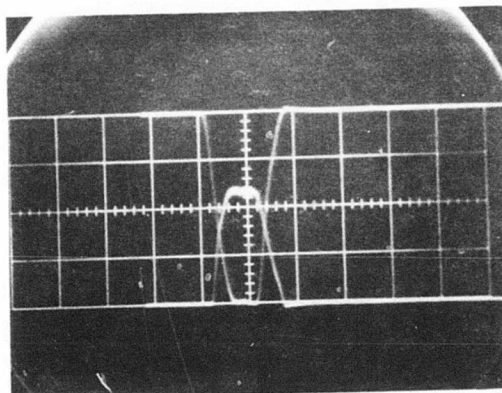
The second factor affecting limitations imposed by facet damage is the pulse duration. It is known from our previous work that the onset of facet damage is dependent on the pulse length; however, data had not been available on devices of interest in the present contract.

We performed a series of experiments using four-heterojunction lasers having (in the notation of Fig. 5) $d_1 = d_5 = 1.13 \mu\text{m}$, $x_1 = x_5 = 0.3$; $d_2 = d_4 = 0.5 \mu\text{m}$, $x_2 = x_4 = 0.2$; $d_3 = 0.2$, $x_3 = 0$. Because of driver limitations, the pulse shape was not quite "square" but did reasonably approximate the desired shape. In Fig. 15 we show the current pulse used to obtain the damage data at each pulse width together with the appearance of the facet after damage. Note that the facet is usually not uniformly damaged, with the edge of the diode frequently (but not always) showing damage first, suggesting the propagation of damage from the edge of the diode inward. The damage data as a function of pulse width are shown in Fig. 16 and indicate a damage limit which is inversely proportional to the square root of the pulse width. Also shown in Fig. 16 are our earlier data for single-heterojunction laser diodes. While having higher limits than the four-heterojunction device tested, the



50 ns/div→

(a)



100 ns/div→

(b)

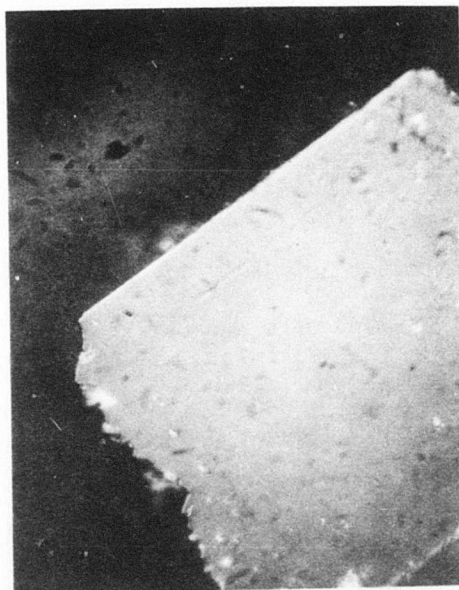
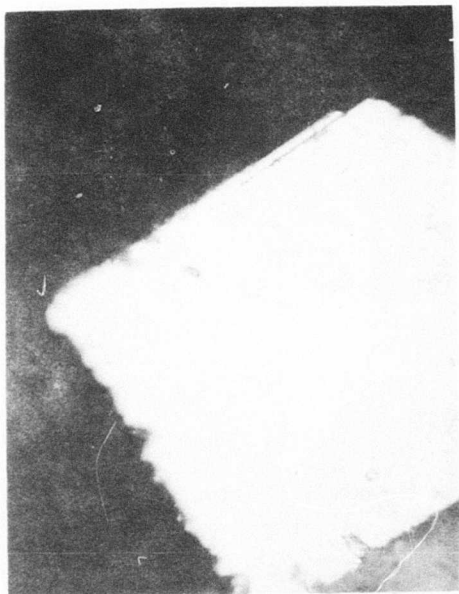
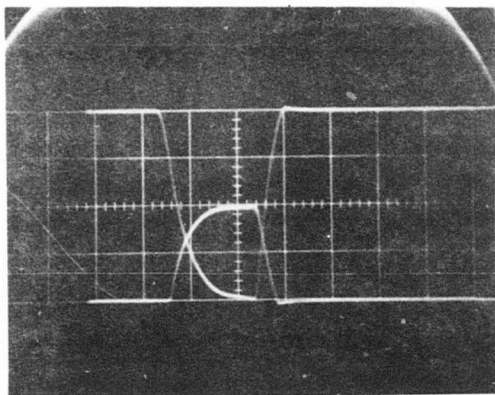
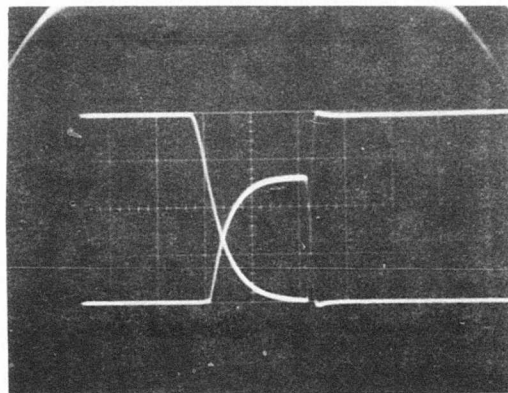


Figure 15. Instantaneous or catastrophic facet damage with pulse width increasing from 50 ns (a) to 2 μ s (f). The photomicrographs (780X) of the facets show the line of damage in the optical cavity.



100 ns/div→

(c)



200 ns/div→

(d)

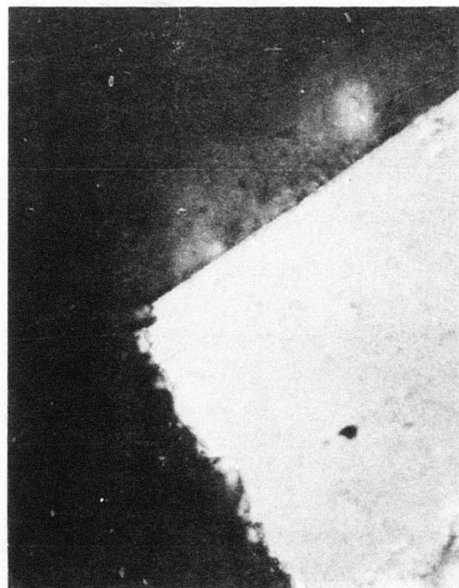
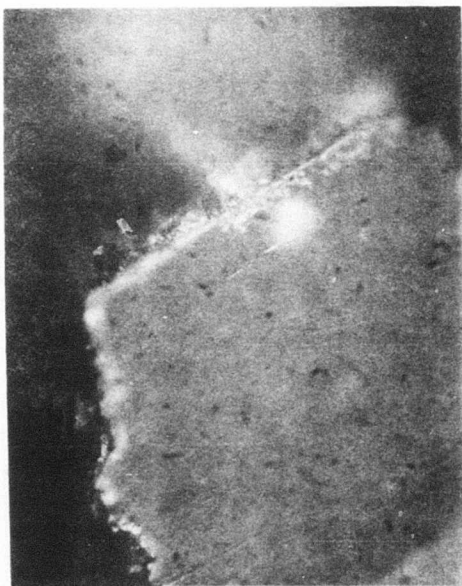
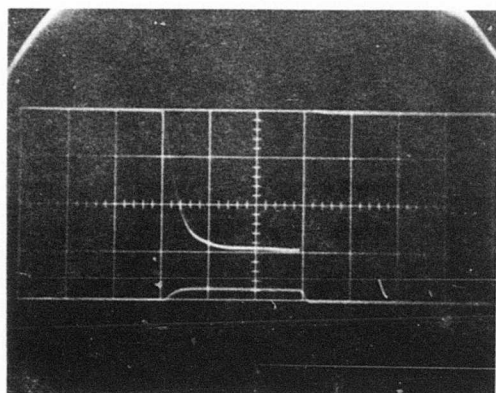
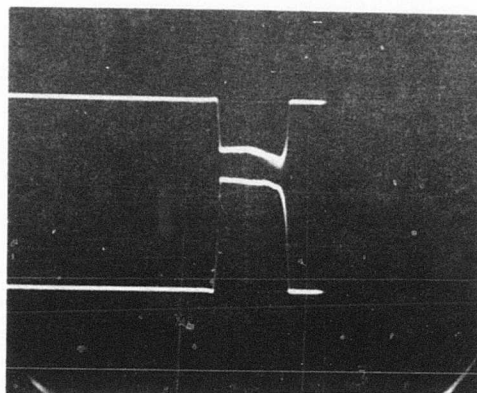


Figure 15. Continued.



200 ns/div→

(e)



.5 μs/div→

(f)

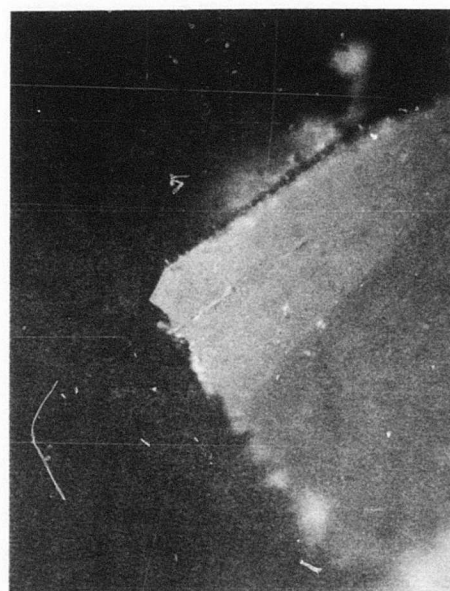
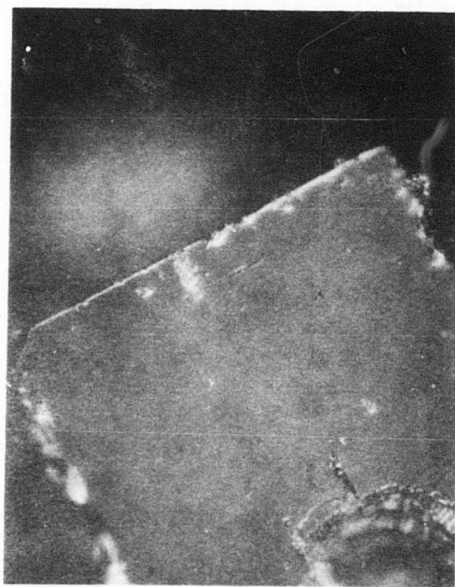
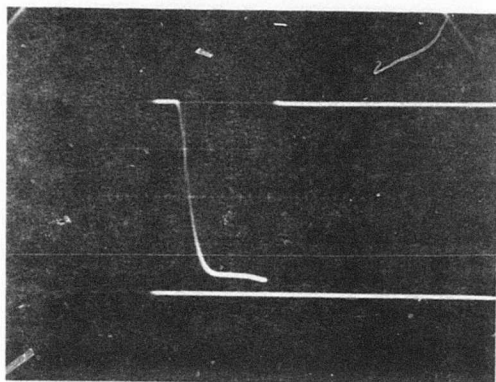
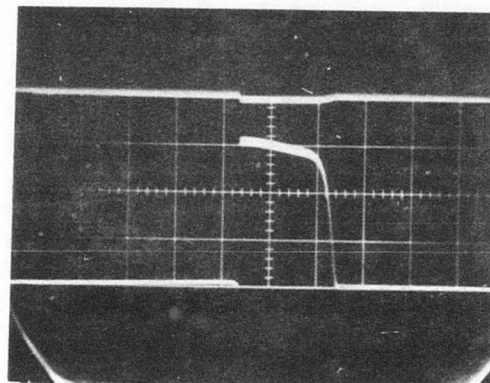


Figure 15. Continued.



0.5 μ s/div

(g)



1 μ s/div

(h)

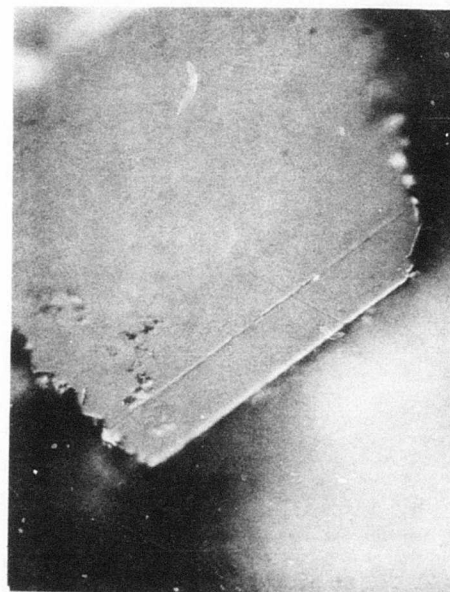
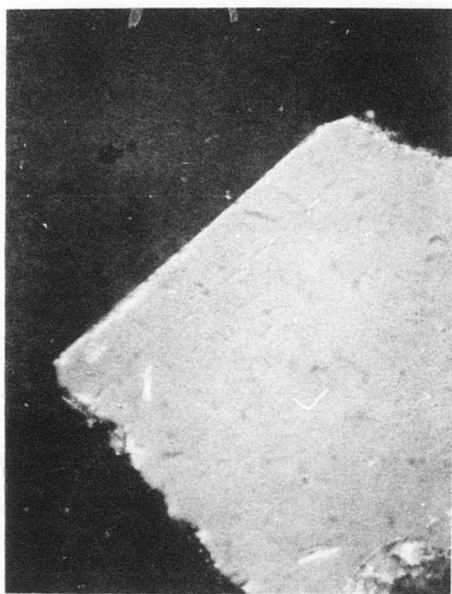


Figure 15. Continued.

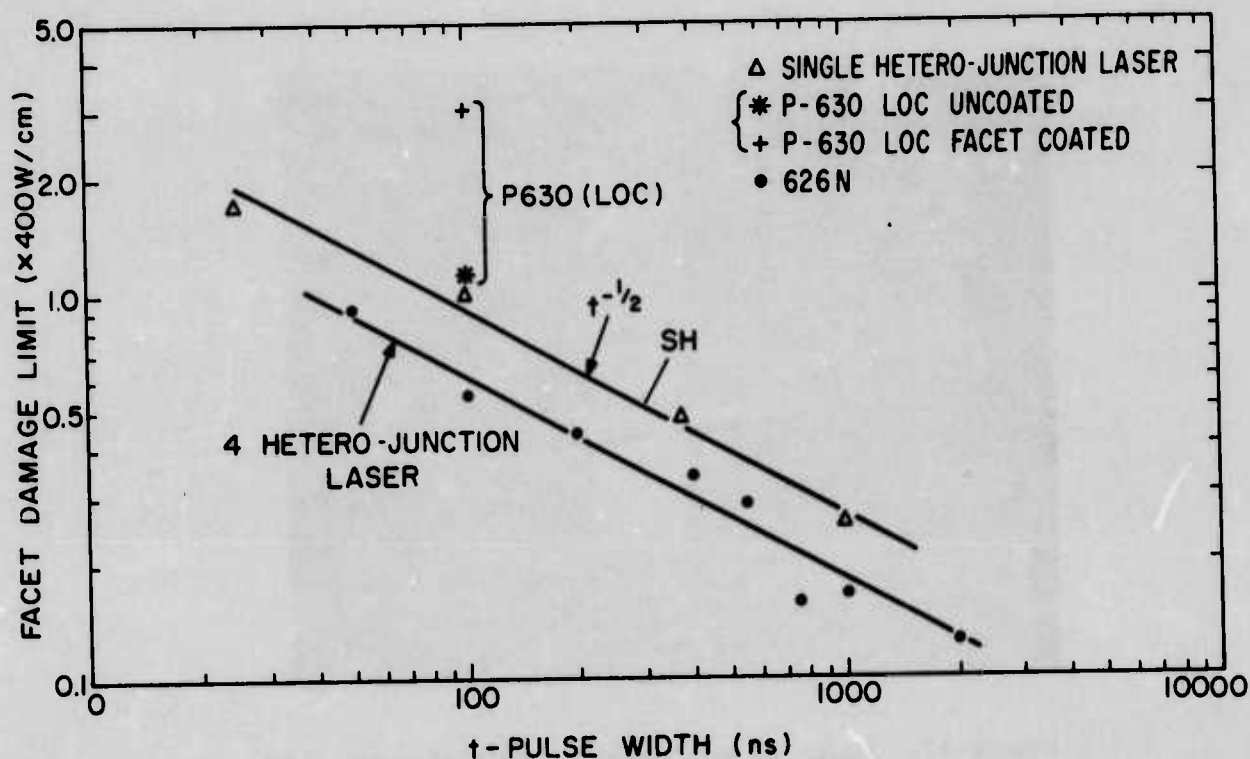


Figure 16. Dependence of facet damage on pulse width for uncoated lasers. The data points for P-630 LOC type lasers are given for coated and uncoated structures and correspond closely to previously obtained data for single-heterojunction lasers (upper curve). The lower curve is data taken on four-heterojunction lasers.

same $t^{-1/2}$ damage limit is indicated. Additional data published for double-heterojunction lasers [15] also suggest the same behavior, therefore indicating that it is possible to extrapolate the damage limit for a wide range of pulse duration values from limited experimental data.

Figure 16 also shows data obtained with a 100-ns-wide pulse on the type of LOC laser delivered under this contract. The uncoated diodes damage at ~ 400 W/cm, comparable to the single-heterojunction diodes. However, after coating with an antireflecting SiO film, the damage limit was increased to 1200 W/cm. Figure 17 shows the facet of the laser damaged at the 1200-W/cm level. The damage starts near a flaw at the edge of the laser and propagates along the facet toward the center. Although this represents a rather high

15. P. G. Eliseev, *Semiconductor Light Emitters and Detectors*, A. Frove, Ed., (North Holland Publishing Co., Amsterdam, 1973).

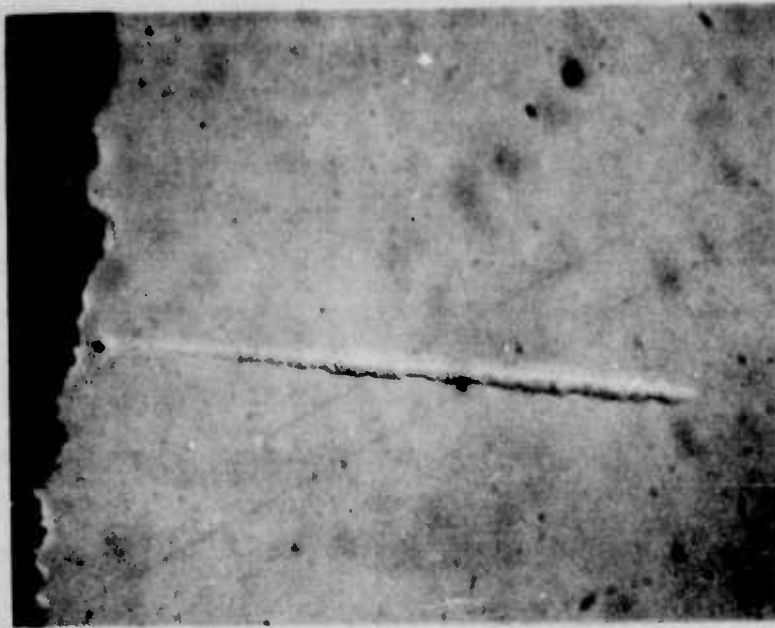


Figure 17. Facet damage observed on high-power LOC laser at the 1200-W/cm operating level. (Facet originally coated with SiO which was removed to obtain this photograph.)

damage limit, it can be anticipated that still *greater* reliability can be achieved with the use of stripe geometry. However, since this is not a current production technique in standard use, the diodes delivered under this contract have sawed sides.

Finally, it should be noted that the instantaneous or catastrophic damage limit serves only as an indication of the upper limit of operation of the laser. For long-term reliability, operation at a considerably lower level is essential. It was not possible to establish good statistics for long-term laser operation since the final diode design evolved late in the contract period. However, it can be said that lasers from the delivered types have been operated at the 400-W/cm level at a repetition rate of 1 kHz with no appreciable drop in output after 350 hours.

D. RADIATION PATTERNS AND BEAM COLLECTION EFFICIENCY

Since one of the goals of this work is to maximize the amount of power collected by f/1.3 optics, data are presented below on power measurements as a function of angular aperture. The unit studied is a LOC-type device with a

cavity width of approximately $2\text{ }\mu\text{m}$. Narrow-beam fundamental-mode operation was achieved by maintaining much lower Al concentrations in the (AlGa)As regions adjacent to the cavity than shown in Table 1. The narrow beam is achieved at the expense of threshold current density and high-temperature performance. Nonetheless, the results are illuminating.

Figure 18 shows the beam profile from a diode with a SiO antireflecting coating on the front facet and, to assure that all measurements refer to the front facet, a coating of black wax on the rear facet. The solid curve is the transverse profile (plane perpendicular to junction) and the dashed curve the lateral profile (in plane of junction) taken at an output power of 300 W/cm . This type of cavity radiates an essentially conical beam with full angle at half intensity of 12° in each plane. The transverse profile has a shape expected for the lowest-order transverse mode. Notice that the coherent pattern persists to -30 dB , where it apparently reaches the background level of the spontaneous emission. This occurs at an angle of only 30° from the normal, which again attests to the remarkably narrow and clean transverse profile.

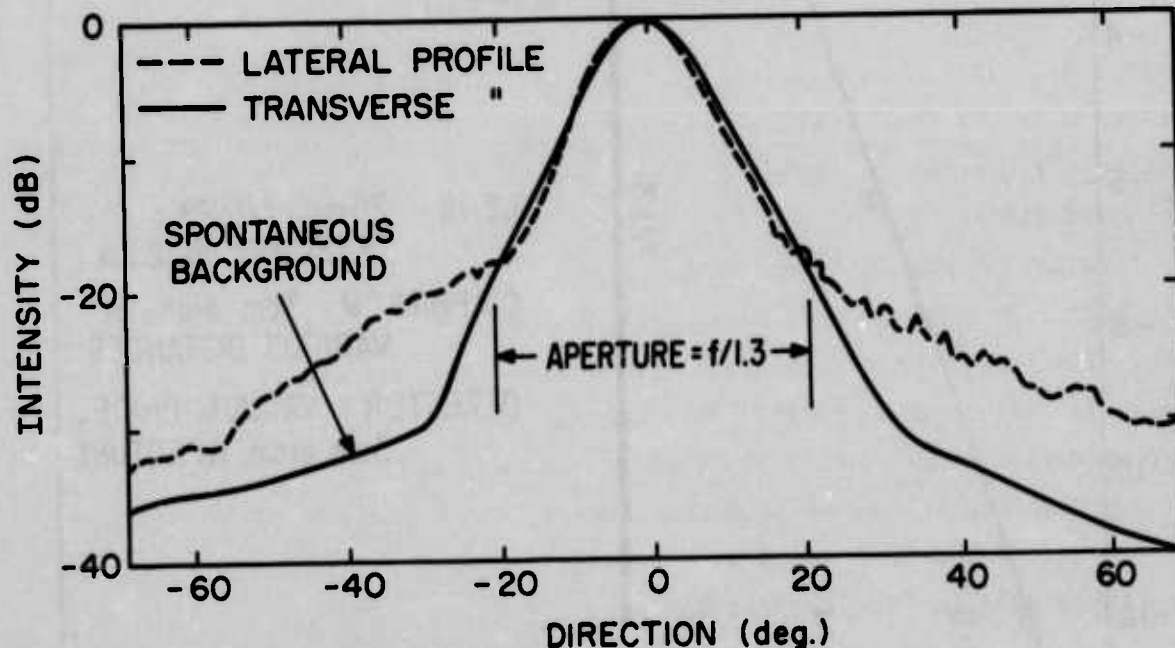


Figure 18. Far-field radiation pattern of narrow-beam LOC laser.

The lateral profile is more conventional, although also very narrow for such a high power output. To -10 dB, it follows the behavior expected for sawed sides and deviates from the predicted sharp cutoff at about $\pm 12^\circ$ in the way found in other units with sawed sides. Although the shoulders in the lateral profile are weak for angles greater than 20° , they still contain enough power to prevent achieving a collection efficiency exceeding 90%.

Figure 19 shows a rough measurement of the losses when the beam is collected with an optical system with limited aperture. The received power in dB is plotted against the numerical aperture of the optical system. The solid curve is measured with a calibrated F-4000 vacuum photodiode having a cylindrical pupil 3 cm in diameter placed 0.7 m from the laser and a 25-mm

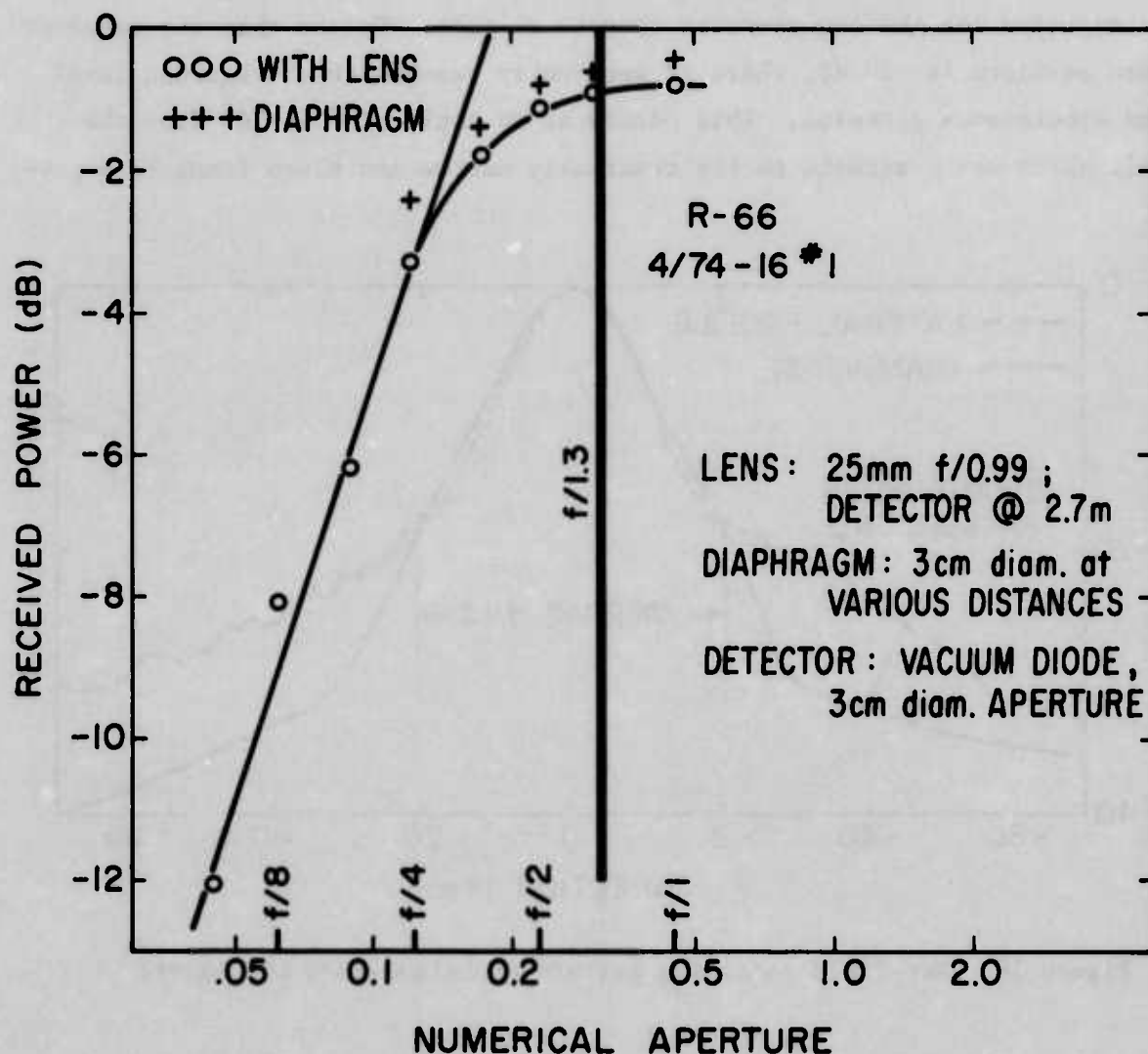


Figure 19. Received power vs. conical collecting angle.

f/1.1 camera lens to project the source onto the detector. For large aperture of the lens, the received power falls only slowly with increase in f number, but by $f/4$ the fall has reached the limiting rate of the reciprocal of the area of the lens opening. The crosses at large aperture are measured without a lens by changing the distance between the laser and the F-4000. They indicate that the insertion loss of the glass in the lens is about 0.5 dB.

Several practical conclusions can be drawn from these results:

- (1) A collection efficiency of 80 to 90% seems possible without unduly expensive optics when the laser beam is 12° wide. This will not be true for the high-temperature lasers delivered under this contract.
- (2) $f/1.3$ optics is essentially as good as a larger aperture lens. It would be cheaper to improve the collection by reducing the insertion loss of the glass with better AR coatings than by increasing the lens size.
- (3) A collection efficiency exceeding 90% requires great attention to the energy in the weak sidelobes of the lateral profile. Extensive study of the mode powering in cavities with sawed sidewalls has failed to reveal either the cause of the weak coherent radiation at large lateral angles (lateral angles greater than 20° in this laser) or a method of suppressing it. *The present state-of-the-art offers no indication that such large collection efficiencies can be achieved.*

The beam patterns of two randomly chosen lasers of the type specifically developed for this contract are shown in Fig. 20. In both cases the half-power (full) beam width perpendicular to the junction plane is 28° . Parallel to the junction plane (not shown), the beam width is less than 15° . There is some difference between the devices at large emission angles so that the amount collected by $f/1.3$ optics (collection angle of 42°) differs. For device A, 75% of the radiation in the perpendicular plane is collected. Since essentially all of the radiation in the parallel plane is collected, this means that 75% of the total radiation will be collected. For device B, somewhat less, 65%, is collected by $f/1.3$ optics. These results are consistent with the discussion above outlining the difficulty of collecting 90% of the emitted power with $f/1.3$ optics.

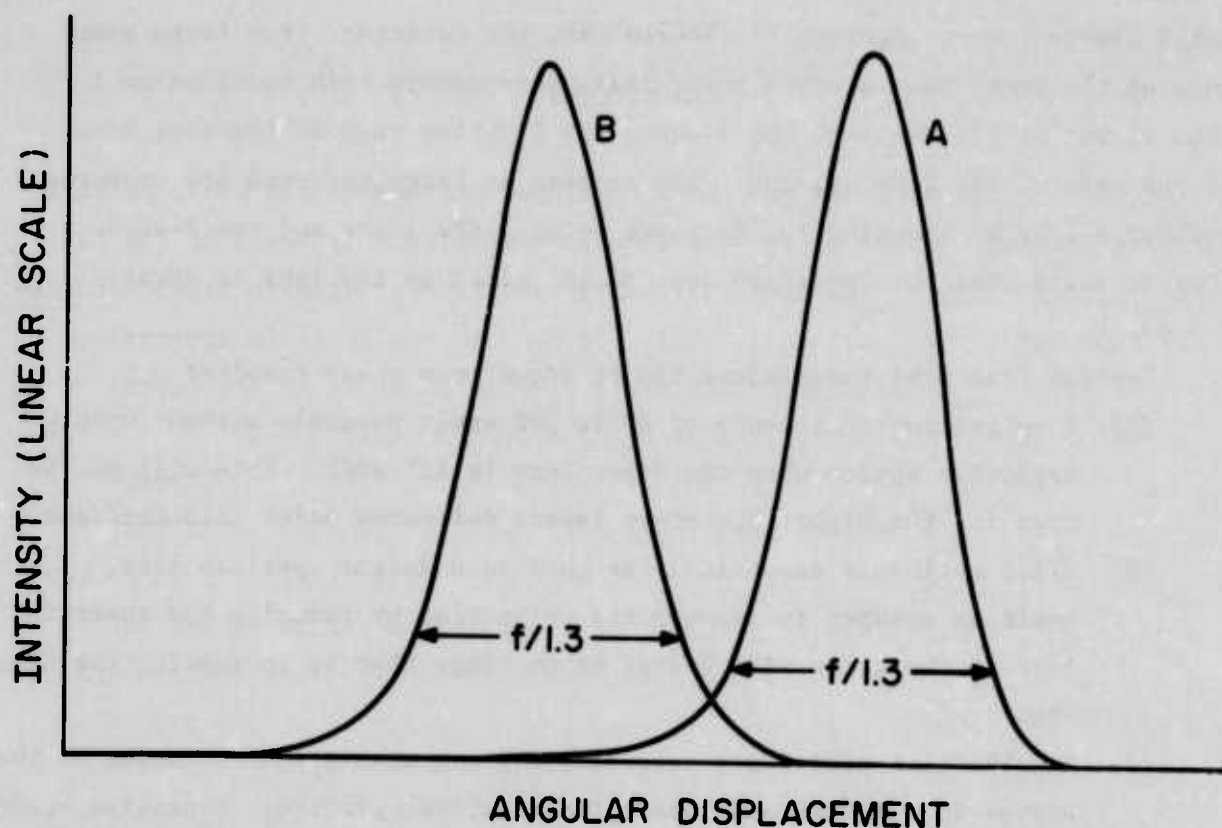


Figure 20. Far-field radiation patterns (perpendicular to junction plane) of two essentially identical laser diodes, both having half-power beam widths of 28° . Diode A was grown at RCA Lancaster and passes 75% of emitted radiation through $f/1.3$ optics (42°). Diode B was grown at RCA Laboratories and passes 65% of emitted radiation through $f/1.3$ optics.

SECTION VI

CONCLUSIONS

High-power laser diodes have been developed which meet the basic requirements for ranging applications. The structure developed is based on the LOC (large optical cavity) heterojunction design and is optimized to provide fundamental transverse mode operation. This has been accomplished by appropriate choice of heterojunction spacing and refractive index steps at the heterojunctions to prevent the propagation of high-order modes.

The devices are designed to be operated continually at a peak power emission level of 400 W/cm of emitting facet. With antireflecting films, they are capable of withstanding up to 1200 W/cm of instantaneous peak power with a 100-ns duration pulse. (A detailed study of the damage threshold dependence on pulse length indicates that the damage threshold decreases with the square root of the pulse length. Hence, failure limits at other pulse length values can easily be estimated.)

These lasers are capable of efficient operation at temperatures in excess of 75°C. The realization of this new structure was made possible by the availability of a sophisticated liquid-phase epitaxial technology developed at RCA Laboratories with which large-area wafers can be grown, having closely controlled dopant composition and layer thicknesses. The technology has been successfully transferred to the RCA Lancaster activity which is responsible for manufacturing laser diodes. Thus, devices, which in every way are equivalent to those obtained under laboratory conditions in Princeton, have been produced under model shop conditions at Lancaster.

The impact of the devices developed under this program is in allowing the eventual high-volume manufacture (with high yields) of structures designed for fusing and other ranging applications. Previously, single-heterojunction lasers have been used for this application. However, the realization of efficient 75°C operation with single-heterojunction lasers requires considerable selectivity in the choice of GaAs substrates, thus introducing a limiting factor in their reproducibility. The quality of present LOC lasers is largely independent of the substrate since all of the active regions are epitaxially grown, and the high-temperature performance is automatically determined by the appropriate control of the growth parameters.

REFERENCES

1. H. Nelson, U.S. Patent No. 3,565,702 (1971).
2. H. F. Lockwood and M. Ettenberg, J. Crystal Growth 15, 81 (1972).
3. M. Ilegems and G. L. Pearson, *Proceedings of Second Int. Symposium on GaAs*, The Inst. of Physics and the Phys. Soc., London, 1969, p. 3.
4. J. K. Butler, J. Appl. Phys. 42, 4447 (1971).
5. H. Kressel, H. F. Lockwood, and J. K. Butler, J. Appl. Phys. 44, 4095 (1973).
6. Zh. I. Alferov, M. V. Andreev, V. I. Korol'kov, E. L. Portnoi, and D. N. Tretyakov, Sov. Phys.-Semicond. 2, 1289 (1969).
7. I. Hayashi, M. B. Panish, P. W. Foy, and S. Sumski, Appl. Phys. Letters 17, 109 (1970).
8. H. F. Lockwood, H. Kressel, H. S. Sommers, Jr., and F. Z. Hawrylo, Appl. Phys. Letters 17, 499 (1970); H. Kressel, H. F. Lockwood, and F. Z. Hawrylo, J. Appl. Phys. 42, 561 (1972).
9. G. H. B. Thompson and P. A. Kirkby, IEEE J. Quantum Electron. 9, 311 (1973).
10. J. K. Butler and H. Kressel, J. Appl. Phys. 43, 3402 (1973).
11. H. Kressel, J. K. Butler, F. Z. Hawrylo, H. F. Lockwood, and M. Ettenberg, RCA Review 32, 393 (1971).
12. Some of these results were presented by the authors at the IEEE Device Research Conference, Boulder, Colorado, June 1973.
13. J. K. Butler, private communication, 1973.
14. T. L. Paoli, B. W. Hakki, and B. I. Miller, J. Appl. Phys. 44, 1276 (1973).
15. P. G. Eliseev, *Semiconductor Light Emitters and Detectors*, A. Frove, Ed., (North Holland Publishing Co., Amsterdam, 1973).